Geochemistry, Geophysics, Geosystems®

RESEARCH ARTICLE
10.1029/2025GC012556

Evolution of the Source Mineralogy and Lithospheric Controls on Magmatism During the Northeast Atlantic Continental Breakup

Emily H. Cunningham[1], Sarah Lambart[1], Pengyuan Guo[2], Sayantani Chatterjee[3], Christian Tegner[4], Autumn Hartley[1], Ashley M. Morris[1], Sverre Planke[5,6], Christian Berndt[7], Carlos A. Alvarez Zarikian[8], Peter Betlem[6,9,10], Henk Brinkhuis[11,12], Marialena Christopoulou[13], Eric C. Ferré[14], Irina Y. Filina[15], Joost Frieling[16,17], Dustin T. Harper[18], Morgan T. Jones[6,19], Jack Longman[20], John M. Millett[5,6,21], Geoffroy T. F. Mohn[22], Reed P. Scherer[23], Natalia Varela[24], Weimu Xu[25], and Stacy L. Yager[26]

[1]MagMaX Laboratory, Department of Geology and Geophysics, University of Utah, Salt Lake City, UT, USA, [2]Institute of Oceanology, Chinese Academy of Sciences, Qingdao, China, [3]Earthquake Research Institute, The University of Tokyo, Bunkyō, Japan, [4]Department of Geoscience, Aarhus University, Aarhus, Denmark, [5]Volcanic Basin Energy Research AS, Oslo, Norway, [6]Department of Geosciences, University of Oslo, Oslo, Norway, [7]GEOMAR Helmholtz Centre for Ocean Research Kiel, Kiel, Germany, [8]Scientific Ocean Drilling, Texas A&M University, College Station, TX, USA, [9]Norwegian Geotechnical Institute, Oslo, Norway, [10]Department of Arctic Geology, University Centre in Svalbard, Longyearbyen, Norway, [11]NIOZ Royal Netherlands Institute for Sea Research, Den Burg, The Netherlands, [12]Department of Earth Sciences, Utrecht University, Utrecht, The Netherlands, [13]Sea-Bird Scientific, Bellevue, WA, USA, [14]Department of Geological Sciences, New Mexico State University, Las Cruces, NM, USA, [15]Department of Earth and Atmospheric Sciences, University of Nebraska, Lincoln, NE, USA, [16]Department of Earth Sciences, University of Oxford, Oxford, UK, [17]Department of Geology, Ghent University, Ghent, Belgium, [18]Department of Geology and Geophysics, University of Utah, Salt Lake City, UT, USA, [19]Department of Ecology, Environment and Geoscience, Umeå University, Umeå, Sweden, [20]Department of Geography and Environmental Science, Northumbria University, Newcastle Upon Tyne, UK, [21]Department of Geology and Geophysics, University of Aberdeen, King's College, Aberdeen, UK, [22]CY Cergy Paris Université, Sorbonne Université, CNRS-INSU, Institut des Sciences de la Terre de Paris, ISTeP, Cergy, France, [23]Department of Earth, Atmosphere and Environment, Northern Illinois University, DeKalb, IL, USA, [24]Department of Environmental Sciences, University of Virginia, Charlottesville, VA, USA, [25]School of Earth Sciences and the Research Ireland Centre for Applied Geosciences, University College Dublin, Dublin, Ireland, [26]Department of Environmental, Geology, and Natural Resources, Ball State University, Munice, IN, USA

Abstract The mid-Norwegian Margin, part of the North Atlantic Igneous Province (NAIP), is a well-studied volcanic rifted margin formed during the breakup between Greenland and Eurasia ~56 Ma, with the largest accumulation of magmatic material hosted by the Vøring Margin section. Despite extensive study in the area, the main controls on magmatic productivity during continental breakup remain debated. To constrain the drivers of breakup magmatism, we developed an inverse Monte Carlo statistical melting model that infers source mineralogy from basalt chemistry. When applied to basalts recently recovered on the Vøring Margin, our results reveal a clear shift in source mineralogy during rifting, with peak magmatism coinciding with clinopyroxene enrichment, despite mantle potential temperatures likely being capped below 1500°C. We also establish that, while the proto-Iceland mantle plume played a role during the emplacement of the NAIP, the main driver for the continental breakup magmatism is lithospheric thinning as a consequence of continent breakup. This study provides new insights into the magmatic and geodynamic evolution of the mid-Norwegian Margin, emphasizing the role of lithospheric refertilization in driving breakup magmatism.

Plain Language Summary The mid-Norwegian Margin is part of the North Atlantic Igneous Province, a region that experienced intense volcanic activity during the opening of the Northeast Atlantic Ocean ~56 Ma. Scientists have long debated why so much magma was emplaced in this area—was it due to an exceptionally hot mantle, or did other geological processes play a role? Using basalts collected during the International Ocean Discovery Program Expedition 396 on the Vøring Margin, offshore Norway, we show that instead of extreme heat, the excess magmatism was primarily triggered by thinning of the lithosphere assisted by moderately elevated mantle temperatures. This work advances our general understanding of how continents break apart and how volcanic margins form.

Key Points:

- We present a new Monte Carlo statistical model for basalt melting to constrain the mantle source mineralogy
- Basalts collected on the Vøring Margin record a strong clinopyroxene enrichment in their source, coinciding with the peak of magmatism
- Excess magmatism was fueled both by plume activity and lithospheric thinning, remobilizing the metasomatized lithosphere and underplate

Supporting Information:

Supporting Information may be found in the online version of this article.

Correspondence to:

E. H. Cunningham,
emily.h.cunningham@utah.edu

Citation:

Cunningham, E. H., Lambart, S., Guo, P., Chatterjee, S., Tegner, C., Hartley, A., et al. (2026). Evolution of the source mineralogy and lithospheric controls on magmatism during the Northeast Atlantic continental breakup. *Geochemistry, Geophysics, Geosystems*, *27*, e2025GC012556. https://doi.org/10.1029/2025GC012556

Received 3 JUL 2025
Accepted 28 DEC 2025

Author Contributions:

Conceptualization: Emily H. Cunningham, Sarah Lambart
Data curation: Emily H. Cunningham, Sarah Lambart, Pengyuan Guo, Sayantani Chatterjee, Christian Tegner
Formal analysis: Emily H. Cunningham, Sarah Lambart
Funding acquisition: Sarah Lambart
Investigation: Emily H. Cunningham, Sarah Lambart, Pengyuan Guo,

1. Introduction

Throughout geologic time, plate tectonic processes have continuously been reshaping and reworking Earth's continents. When these processes cause continents to break up, the resulting new continents are each left with conjugate passive margins that broadly record the rifting process. The focus of this study is the mid-Norwegian Margin, a prime example of an excess-magma margin. Excess-magmatic margins, also called volcanic rifted margins, occur where magmatic productivity exceeded what is expected from simple decompression melting without a thermal anomaly (e.g., Franke, 2013; Huismans & Beaumont, 2011, 2014; Lu & Huismans, 2021; Péron-Pinvidic et al., 2019).

Basalts emplaced on the mid-Norwegian Margin are considered part of the North Atlantic Igneous Province (NAIP). The NAIP is one of the largest and best-studied large igneous provinces of the Phanerozoic (Ernst et al., 2021). It consists of extensive flood basalt provinces and associated intrusions and dykes extending over a vast area that includes East and West Greenland, the Faroe Islands, the Norwegian continental margin, Rockall Bank, and the British Isles (Figure 1; Saunders et al., 1997; Storey, Duncan, & Swisher, 2007) and was emplaced during the Paleocene/Early Eocene (Storey, Duncan, & Tegner, 2007; Wilkinson et al., 2017).

Emplacement of the NAIP started ~61 Ma, but the main phase of magmatism coincides with the continental breakup between Greenland and Eurasia (Storey, Duncan, & Tegner, 2007), beginning ~56 Ma. The offshore magmatic deposits of the Northeast Atlantic, and the eastern arms of the NAIP, have been the focus of many ocean drilling expeditions, including Deep Sea Drilling Project (DSDP) Leg 38 (Talwani et al., 1976), Ocean Drilling Project (ODP) Legs 104 (Eldholm et al., 1987), 152 (Larsen et al., 1994), and 163 (Duncan et al., 1996) and more recently, the International Ocean Discovery Program (IODP) Expedition 396 (Planke et al., 2023a). Here, we focus on basalts collected during this latest expedition on the Vøring segment of the mid-Norwegian Margin, which presents the largest accumulation of magmatic material along mid-Norway's continental margin.

IODP Expedition 396 set out to investigate three main hypotheses for the emplacement of the Vøring Margin volcanics: (a) Magmatic production was increased due to elevated mantle potential temperatures resulting from interaction with the proto-Iceland mantle plume (e.g., Morgan, 1971; Saunders et al., 1997; Spice et al., 2016; White & McKenzie, 1989). (b) A tectonic-driven process such as small-scale convection at the base of the lithosphere (e.g., King & Anderson, 1995, 1998), or an early rupture of the lithospheric mantle (e.g., Lu & Huismans, 2021) could have caused an increase of mantle and magma fluxes. (c) The mantle source during rifting was particularly fertile, lending to an unusually productive source region (e.g., Foulger et al., 2005; Korenaga, 2004). Additional hypotheses, such as the contribution of a volatile-rich component or the delamination of the continental lithosphere, have also been proposed (e.g., Gernon et al., 2022; Gorczyk & Gonzalez, 2019; Petersen et al., 2018).

Due to the NAIP's proximity to Iceland, the role of the Icelandic mantle plume in the formation of the NAIP has been investigated for decades (e.g., Lawver & Müller, 1994; Ribe et al., 1995; Saunders et al., 1997; Schilling, 1991; Skogseid et al., 2000; Tegner et al., 1998; Vogt, 1983; White, 1988; Wolfe et al., 1997). The presence of a mantle plume beneath Iceland is supported by the elevated $^{3}He/^{4}He$ isotopic signatures (Brandon et al., 2007; Kurz et al., 1985) and by seismic data (Bijwaard & Spakman, 1999; Celli et al., 2021; French & Romanowicz, 2015; Holbrook et al., 2001; Wolfe et al., 1997). The geochemistry of the Icelandic basalts has also been attributed to the ridge interacting with a mantle plume (e.g., Breddam et al., 2000; Fitton et al., 1997; Murton et al., 2002; Schilling, 1973). The broader NAIP volcanics possess chemical signatures similar to Icelandic basalts (Fitton et al., 1997; Korenaga & Kelemen, 2000; Saunders et al., 1997; Schilling, 1973), including elevated $^{3}He/^{4}He$ isotopic signatures (Marty et al., 1998; Starkey et al., 2009; Willhite et al., 2019), which supports the presence of the proto-Iceland plume during the emplacement of the NAIP.

Small-scale convection has also been suggested as a possible mechanism for high magmatic flux in volcanic rifted margins (e.g., Boutilier & Keen, 1999). Unlike a mantle plume, small-scale convection can potentially operate without significantly elevated potential temperatures, and convective instabilities at the base of the lithosphere are inherently connected to and produced by the rifting process (Keen & Boutilier, 2000). Mutter et al. (1988) first suggested that small-scale convection induced by lateral temperature gradients may provide an enhanced flux of material into the region of partial melting, thereby increasing magmatic activity in the absence of mantle potential temperatures elevated by an external influence. While this hypothesis has attracted some attention (e.g., Boutilier & Keen, 1999; Keen & Boutilier, 2000; Nielsen & Hopper, 2004; Simon et al., 2009), the relative

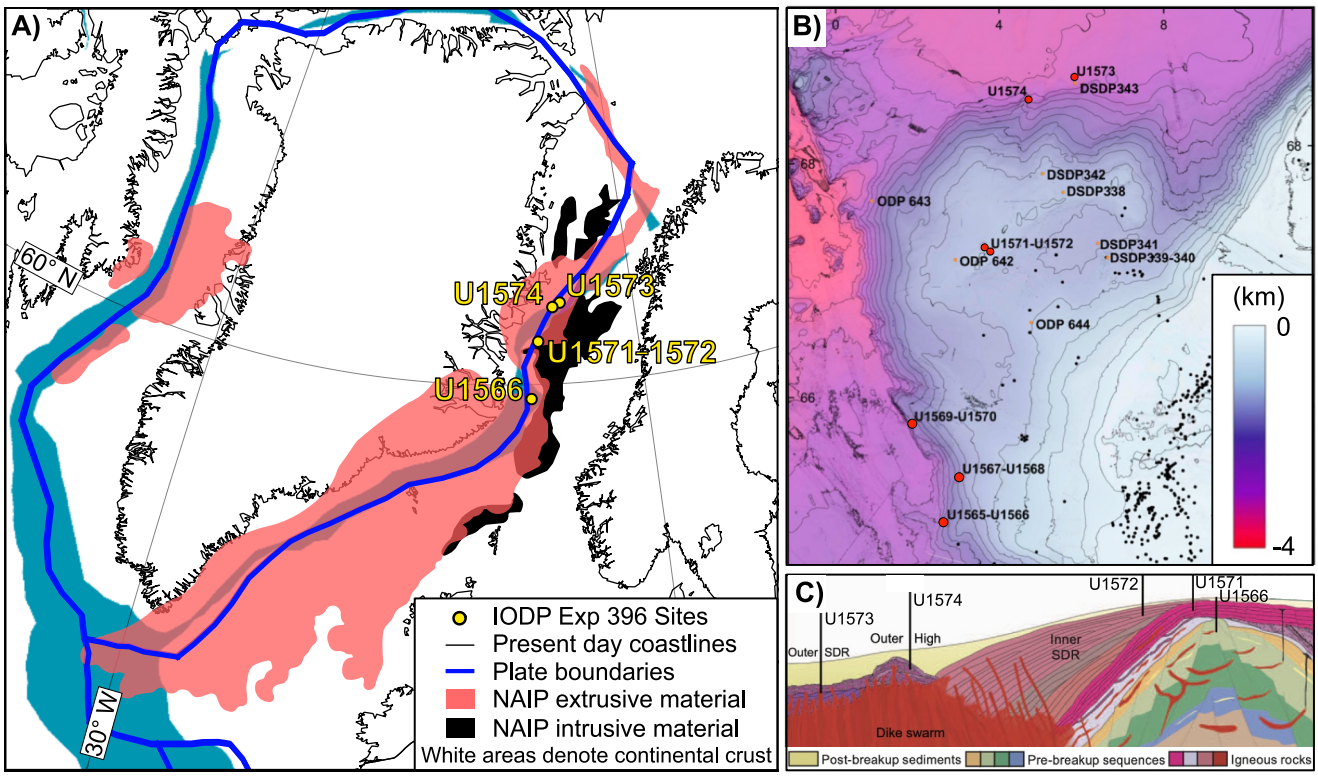

Figure 1. Geologic setting of the study area. (a) Plate reconstruction at 56 Ma depicting the extent of the NAIP extrusive (Jones et al., 2016) and intrusive (Planke et al., 2005; Rateau et al., 2013; Reynolds et al., 2017) deposits, as well as the locations of sites of interest in this study at the time of eruption. Plate reconstruction was made using GPlates (Boyden et al., 2011; Gurnis et al., 2012) following Jones et al. (2023) using the reconstruction model of Zahirovic et al. (2022). (b) Bathymetric map of the Vøring Margin where the drilling locations during IODP Expedition 396 are shown in red. The previous ODP/DSDP sites (orange dots) and industry boreholes (black dots) are shown for comparison. (c) Schematic cross-section through a volcanic passive margin with the locations of sites investigated in this study. SDR: Seaward Dipping Reflectors. Panels (b) and (c) modified from Planke et al. (2023a).

importance of active upwelling in the evolution of rifted volcanic margins is still debated (Holbrook et al., 2001; Koptev et al., 2021; Korenaga et al., 2000, 2002). More recently, Lu and Huismans (2021) used a numerical approach to argue that magma production is correlated with the width of magmatic margins. They concluded that the emplacement of the NAIP could be accounted for via a relatively modest positive thermal anomaly (50–80°C) coupled with depth-dependent extension in which the lithospheric mantle ruptures before the crust.

Finally, Northeast Atlantic basalts are chemically and isotopically heterogeneous, both in space and in time (from the onset of NAIP emplacement through the present magmatic activity in Iceland), implying both changes in the melting conditions (e.g., Fram & Lesher, 1993; Saunders et al., 1997; Tegner et al., 1998) and long-lived heterogeneity in the NAIP mantle source. For example, low $^{143}Nd/^{144}Nd$, and high $^{87}Sr/^{86}Sr$ and $^{208}Pb/^{204}Pb$ ratios are commonly associated with recycled material in the mantle source (e.g., Chauvel & Hémond, 2000; Kent et al., 2004; Shorttle et al., 2014; Thirwall et al., 2004). For this isotopic heterogeneity to appear in the basalts, the length scale of the mantle heterogeneity must be sufficient to survive mechanical mixing, diffusion, and melt mixing. Consequently, it has also been proposed that the mantle source for the NAIP contains lithological heterogeneity, including fertile lithologies (i.e., pyroxenites) that could have contributed to the high magmatic activity (e.g., Brown & Lesher, 2014; Sobolev et al., 2007). However, the nature of this lithological heterogeneity is debated, and Hole (2018) argued against a significant role of pyroxenite in the emplacement of the NAIP.

Though there is still an ongoing debate regarding the nature of the mantle source of the mid-Norwegian Margin basalts and its link with the Iceland plume, many now seem to agree that the emplacement of the NAIP requires some combination of the three main hypotheses described above (e.g., Brown & Lesher, 2014; Hole & Natland, 2020; Koptev et al., 2021; Tegner et al., 1998).

In this paper, we used the compositions of the basalts collected during IODP Expedition 396 to deduce the mineralogy of the mantle source during the formation of the Vøring Margin and provide insights into the cause of excess melting on the mid-Norwegian Margin.

2. Geologic Setting and Basalt Compositions

IODP Expedition 396 collected basalts from the mid-Norwegian Margin, part of the NAIP. The NAIP is one of four large igneous provinces (LIPs) formed during the opening of the Atlantic Ocean. Other Atlantic LIPs include the Central Atlantic Magmatic Province (Marzoli et al., 2018), the Paraná-Etendeka province (Gomes & Vasconcelos, 2021), and the Equatorial Atlantic Magmatic Province (Oliveira et al., 2025). Continental breakup of Eurasia and Greenland prior to the Paleocene–Eocene boundary marked the apex of the periodic but predominantly extensional tectonics in the North Atlantic since the end of the Caledonian orogeny (Meyer et al., 2009; Skogseid et al., 2000). Onshore deposits of the volcanic activity that accompanied the rifting and margin formation in the Northeast Atlantic have long been recognized (e.g., Hutton, 1788; Wilkinson et al., 2017, and references therein). Sea floor deposits of the NAIP were first recovered during the ODP Leg 104 on the Vøring Margin (Figure 1), followed by Legs 152 and 163 off the southeast of Greenland (e.g., Larsen et al., 1999; Saunders et al., 1998). These magmatic events prior to and during continental separation, and the ongoing activity of Iceland, comprise the NAIP. A large accumulation of magmatic material is found on the Vøring Plateau, where drilling was conducted during IODP Expedition 396 (Figure 1).

Sites referenced in this work (U1566, U1571, U1572, U1573, and U1574) represent the locations where basaltic rocks were recovered during Expedition 396. These sites are believed to sample the evolution of a volcanic margin with time: from Landward Flows interpreted as subaerial or shallow marine flood basalts and representing the initiation of rifting (Site U1566; Planke et al., 2023b), to Inner Seaward Dipping Reflectors (SDR) representing subaerial flood basalts emplaced during the peak of magmatic activity (Sites U1571 and U1572; Planke et al., 2023c), to the transition to a marine environment with emplacement at shallow depths (Site U1574; Planke et al., 2023d), and in a deep marine depositional environment (Site U1573; Planke et al., 2023e) (Figure 1). The geologic context of each site with respect to the rifting process was inferred prior to the expedition using detailed seismic surveys and the long history of scientific and industry drilling data that have been collected on the mid-Norwegian Margin (Planke et al., 2023a).

The SDR sequence has been previously drilled in Hole 642E by Ocean Drilling Project Leg 104 (Eldholm et al., 1989) on the Vøring Margin. Companion Sites U1571 and U1572 were drilled near the location of Hole 642E with the goal of more completely sampling the SDR sequence. Though Sites U1571 and U1572 show distinct morphology in seismic surveys due to differences in weathering (Planke et al., 2023c), the basalts sampled at each site are geochemically similar. Therefore, Sites U1571 and U1572 will be discussed together throughout this work (i.e., U1571-U1572).

Detailed petrography of the basaltic samples is reported in the expedition reports (Planke et al., 2023b, 2023c, 2023d, 2023e), and Text S1 in Supporting Information S1 provides a brief summary of the samples collected at each site. The vast majority of basalts recovered during the expedition were aphyric basalts with minor sections of plagioclase phyric basalts. While the age of basaltic basement at each site has not yet been precisely determined, several pieces of evidence (see Text S1 in Supporting Information S1) indicate that basalts at Site U1566 were emplaced in the late Paleocene, while basalts recovered from the other sites were emplaced in the Early Eocene.

Compositions of the basalts used in this study are reported in Table S1 and presented in Figure S1 in Supporting Information S1 (see Appendix A for analytical methods). Heavily altered samples, that is, those with high loss on ignition (LOI > 5 wt.%), and highly fractionated basalts (MgO content < 5 wt.%), are not included in this study. Overall, basalts at Site U1566 show a relatively limited MgO range, between 7.8 and 9.4 wt.%, SiO_2 contents between 47.6 and 51.1 wt.%, CaO/Al_2O_3 ratios between 0.61 and 0.78, and low alkali ($Na_2O + K_2O$) contents (2–2.6 wt.%) (Figure S1 in Supporting Information S1). Major element compositions of basalts at Site U1573 are similar to the basalts from Site U1566, with slightly higher Na_2O and SiO_2 contents and lower CaO contents. At Site U1574, the basalts are slightly more primitive (8.1–9.9 wt.% MgO) and show slightly higher SiO_2 and alkali content than U1566 basalts. Finally, basalts at Site U1571/72 have lower MgO contents than at other sites. They are also richer in TiO_2, P_2O_5, Na_2O, and K_2O, consistent with a higher degree of fractionation. However, a simple modeling of fractionation crystallization of ol, cpx and pl cannot produce U1571-1572 samples from the high-MgO U1566 samples, potentially indicating a difference in mantle source.

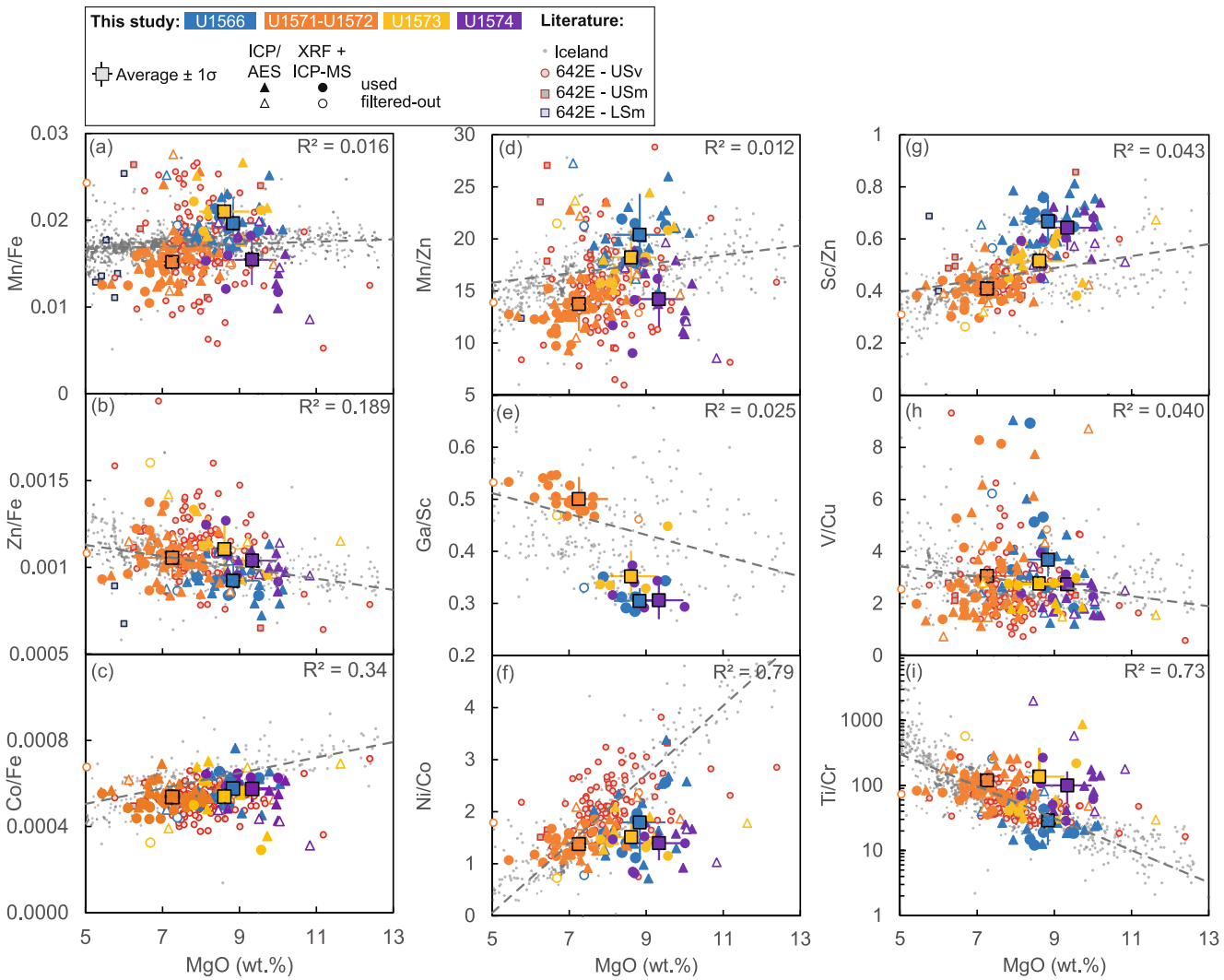

Figure 2. Element ratios as a function of the MgO (wt.%) content of the basaltic samples collected during IODP Exp. 396. The dashed gray lines and the associated R^2 correspond to the linear (a–h) and exponential (i) best-fit calculated on samples from Iceland (Harðardóttir et al., 2022).

Elemental ratios for each site broadly follow trends for Iceland and are largely similar to basalts from Site 642E, though with some key differences (Figure 2). U1571-U1572 basalts show the lowest Mn/Fe, Mn/Zn, and Sc/Zn ratios, but mostly differ from other sites by their high Ga/Sc ratios. In contrast, for a given MgO content, U1566 basalts are characterized by high Sc/Zn, Mn/Fe, Mn/Zn, V/Cu, and Ni/Co ratios and low Zn/Fe, Ga/Sc, and Ti/Cr ratios. U1573 basalts present the highest average Mn/Fe, but other ratios are intermediate with the values obtained for the other sites. Finally, U1574 basalts have ratios similar to those of the U1571-U1572 basalts, except for Ga/Sc and Sc/Zn ratios that are similar to those of U1566 basalts.

3. Nature of the Mantle Source

We considered constraining the mantle potential temperature (T_P) an appropriate first step toward understanding the melting conditions of the Vøring Margin basalts. PRIMELT3 (Herzberg & Asimow, 2015) is a popular choice for estimating T_P; however, this software is only able to correct for olivine fractionation and assumes that basalts derive from an anhydrous peridotite source. If the basalt compositions are not consistent with such assumptions, the software provides warning flags to indicate it cannot provide an accurate T_P. When applied to the basalts collected during IODP Expedition 396 (see Text S2 in Supporting Information S1), all but one calculation using IODP Expedition 396 basalts resulted in the warning flag "pyroxenite source." In PRIMELT3, low CaO content for a given MgO content is used as evidence for a melt produced by pyroxenite (Herzberg & Asimow, 2008).

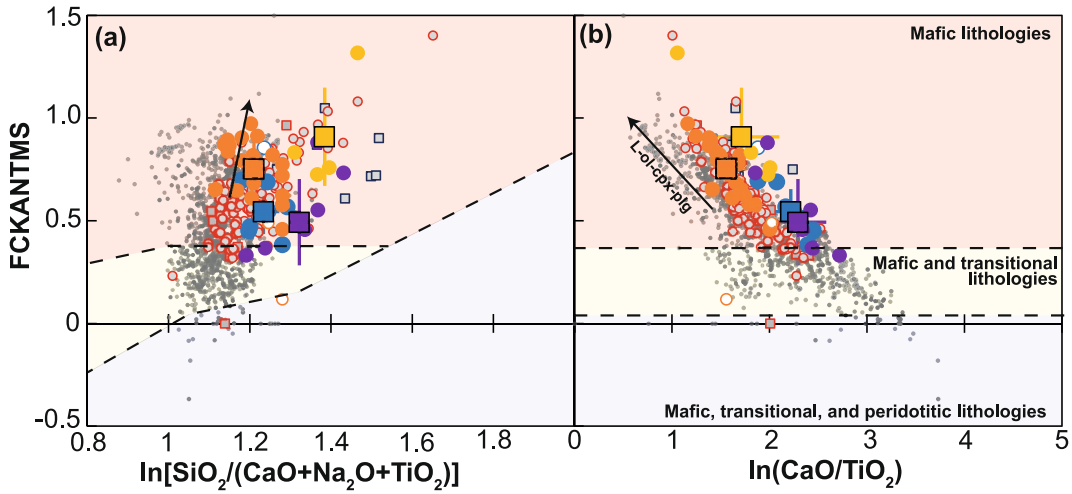

Figure 3. FCKANTMS plots. FCKANTMS (=ln(FeO/CaO) – 0.08 × ln(K_2O/Al_2O_3) – 0.052 × ln(TiO_2/Na_2O) – 0.036 × ln(Na_2O/K_2O) × ln(Na_2O/TiO_2) – 0.062 × $(\ln(MgO/SiO_2))_3$ – 0.641 × $(\ln(MgO/SiO_2))_2$ – 1.871 × ln(MgO/SiO_2) – 1.473, in wt.%), versus (a) ln(SiO_2/(CaO + Na_2O + TiO_2)) and (b) ln(CaO/TiO_2) for basalts from Expedition 396 compared with a sample compilation from Iceland (Harðardóttir et al., 2022) and basaltic samples from ODP Hole 642E (Meyer et al., 2009; Viereck et al., 1989). The color and symbol code are the same as in Figure 2. Black arrows marked with L-Ol-Cpx-Pl, fractional crystallization trends of olivine, clinopyroxene, and plagioclase. The colored fields describe melts derived from different lithologies (Yang et al., 2019).

However, the range of pyroxenite compositions is large, and not all pyroxenites will necessarily generate melts with low CaO content for a given MgO content (Lambart et al., 2013). Similarly, peridotite melts can also have low CaO content (e.g., Yang & Zhou, 2013). Thus, a CaO-MgO discriminant line cannot be used alone to distinguish between pyroxenite melts and peridotite melts.

To assess the presence of lithological heterogeneity in the mantle of the Vøring Margin, we used the "FCKANTMS" parameter proposed by Yang et al. (2019). FCKANTMS is based on log ratios of major and minor elements in basalts to discriminate between mafic, peridotitic, and transitional (i.e., olivine-bearing pyroxenites) lithologies in the mantle source. The authors argue that fractionation, variation of pressure and temperature conditions, or the presence of volatiles in the source all have little to no impact on this parameter. When applied to basalts collected from Expedition 396, most samples plot in the mafic lithology field, suggesting that the composition of the basalts could not have been produced from melting of peridotite without the contribution of a mafic or recycled component (Figure 3). However, the nature of the mafic (or transitional) component is not defined, and the discriminating plots in Figure 3 cannot be used to quantify the proportion of this component in the mantle source. Considering the preliminary interpretations of sites sampled during Expedition 396 (i.e., U1566 representing the onset of rifting while U1571-U1572 represents the peak of magmatism), the mass fraction of the mafic component in the source may vary between sites.

Over the past two decades, First Row Transition Elements (FRTEs) have been suggested as potential tracers of lithological or mineralogical heterogeneity of the mantle source (e.g., Bowman & Ducea, 2023; Cao et al., 2022; Davis et al., 2013; Gómez-Ulla et al., 2017; Herzberg, 2011; Howarth & Harris, 2017; Humayun et al., 2004; Le Roux et al., 2010, 2011, 2015; Mallik et al., 2021; Mourey et al., 2022; Prytulak & Elliott, 2007; Qin & Humayun, 2008; Sobolev et al., 2005, 2007; Straub et al., 2008; Xu et al., 2020). FRTEs are thought to be good tracers for mantle lithological heterogeneity due to their compatible to slightly incompatible nature within the main mantle minerals, causing their ratios to be minimally affected by fractionation and metasomatic processes (Humayun et al., 2004; Le Roux et al., 2010). Gallium is often associated with FRTEs due to its similar partitioning behavior (Davis et al., 2013). As a consequence, concentrations (e.g., Ni, Mn) or ratios (e.g., Mn/Fe, Zn/Fe, Ga/Sc) of FRTEs + Ga have been used to discriminate between magma derived from peridotite and pyroxenite sources (e.g., Bowman & Ducea, 2023; Gurenko et al., 2009; Le Roux et al., 2011; Sobolev et al., 2005, 2007). However, one of the main limitations of this approach is that pyroxenites and peridotites form a continuous spectrum of mineralogy and composition (e.g., Herzberg, 2011; Kogiso et al., 2004; Lambart et al., 2013) rather than two distinct populations. Hence, using FRTEs + Ga to discriminate between peridotite and pyroxenite source

requires assumptions about the mineralogy and composition of each lithology. In addition, Lang and Lambart (2022) showed that a single FRTE ratio in a basalt can be reproduced by a large range of bulk source mineralogies. They proposed that the source mineralogy may however be constrained by using a combination of two (or more) FRTE ratios. Here, we build on the proof of concept presented by Lang and Lambart (2022) and use five elemental ratios (Mn/Fe, Zn/Fe, Mn/Zn, Sc/Zn, and Ga/Sc) to constrain the source mineralogy of the basalt samples collected during IODP Expedition 396. Below, we describe the modeling approach and the reasoning for the choice of the elemental ratios used in the model. Through these modeling efforts, we aim to advance our understanding of the evolution of the mantle source throughout the rifting process.

3.1. Modeling Approach

Rather than assuming the nature of the different lithologies potentially present in the mantle, Lang and Lambart (2022) proposed a new approach to determine the bulk mineralogical make-up of the mantle using FRTE ratios. Applying this model to basalt suites from the Western Volcanic Zone (WVZ) in Iceland and Samoa, they demonstrated that the two oceanic islands show contrasted bulk mineralogy with the melt source of Samoa being more enriched in garnet and olivine than the melt source of Iceland. However, their model was a proof of concept as they only considered two elemental ratios (Mn/Fe and Zn/Fe), the basalt suites were deliberately chosen for having contrasted Mn/Fe and Zn/Fe ratios, and the variability of the basalt composition at each location was not taken into account. We have expanded upon their findings by using a Monte Carlo statistical model that calculates the bulk mineral assemblages capable of reproducing five elemental ratios observed in basalts. In this section, we describe the numerical approach.

In our calculations, model inputs are the elemental ratios measured in the basalts (represented by R_B) and their respective standard deviations (σ_{R_B}) for each site. Other parameters include the partition coefficients of each element of interest (Table S2), the melt fraction (F; see Appendix B), the number of bulk mineralogies to be tested (n), and the corresponding elemental ratios in the mantle source (R_0; see Appendix C).

Elemental ratios of the liquid (R_L) for each source mineralogy are calculated using the modal aggregated fractional melting equation, shown below for the Mn/Fe ratio:

$$R_{L\ \mathrm{Mn/Fe}} = R_{0\ \mathrm{Mn/Fe}} \times \frac{1-(1-F)^{1/D_{0\mathrm{Mn}}}}{1-(1-F)^{1/D_{0\mathrm{Fe}}}}, \quad (1)$$

where $R_{L\mathrm{Mn/Fe}}$ is the Mn/Fe ratio in the liquid, $R_{0\mathrm{Mn/Fe}}$ is the Mn/Fe ratio of the source, $D_{0\mathrm{Mn}}$ and $D_{0\mathrm{Fe}}$ are the bulk partition coefficients for these elements, and F is the melt fraction. Bulk partition coefficients are calculated with the mineral-melt partition coefficients listed in Table S2 and weighted with respect to the fraction of each mineral (X) for a given bulk mineralogy. We consider 5 minerals to make up the mantle bulk rock: garnet (grt), olivine (ol), clinopyroxene (cpx), orthopyroxene (opx), and spinel (sp). For the first run of the model, each mineral fraction can vary between 0 and 1, except for spinel which, as an accessory mineral, is only varied between 0 and 0.1. The mineral abundances are then normalized to ensure that the sum of the mineral fractions is always 1. Additional calculations can be run by refining the constraints on the mineral mode based on this initial calculation so that the mineralogy space can be better covered for the same number of runs.

To account for the compositional variability of the basalts at each site, we used the average elemental ratios at each site, R_B, and their associated standard deviations. We then compare the calculated R_L values to the natural R_B values and select the bulk mineralogies as follows:

$$\mathrm{Res} = (R_L - R_B)^2 \leq (\sigma_{R_B})^2, \quad (2)$$

where Res is the residual value.

We can also calculate the squared residual BulkRes, such as:

$$\mathrm{BulkRes} = \Sigma \frac{\mathrm{Res}}{{R_B}^2} \quad (3)$$

Table 1
Basalt Element Ratios

	U1566	U1571-U1572	U1573	U1574	WG[a]	Source[b]
Mn/Fe	**0.0196 (30)**	**0.0152 (27)**	**0.0210 (28)**	**0.0155 (29)**	**0.0168 (14)**	**0.0167 (31)**
Zn/Fe	**0.000925 (95)**	**0.00106 (12)**	**0.00111 (15)**	**0.00104 (11)**	**0.00103 (12)**	**0.00092 (13)**
Mn/Zn	**20.4 (39)**	**13.7 (26)**	**18.2 (27)**	**14.2 (29)**	**16.6 (23)**	**18.2 (42)**
Sc/Zn	**0.664 (79)**	**0.409 (55)**	**0.515 (80)**	**0.643 (86)**	**0.397 (78)**	**0.314 (61)**
Ga/Sc	**0.305 (24)**	**0.501 (43)**	**0.352 (49)**	**0.306 (37)**	**0.503 (95)**	**0.247 (46)**
Ni/Co	1.79 (66)	1.38 (24)	1.51 (27)	1.40 (33)	7.1 (41)	17.8 (34)
Co/Fe	0.00058 (7)	0.00054 (5)	0.00054 (12)	0.00058 (6)	0.00087 (19)	0.00155 (24)
V/Sc	6.20 (62)	8.73 (74)	7.83 (95)	6.62 (70)	8.57 (141)	5.35 (88)
Ti/Cr	29 (17)	119 (70)	140 (24)	100 (64)	37 (72)	0.72 (32)
V/Cu	3.7 (19)	3.1 (18)	0.33 (3)	2.7 (6)	3.5 (36)	2.9 (5)

Note. Elemental ratios of basalts (R_B) used during model calculations for Sites U1566, U1571-U1572, U1573 and U1574 (IODP Expedition 396) and West Greenland (WG), and source element ratio (R_0), with associated one standard deviation. The ratios used in the Monte Carlo model are in bold. The error (in parentheses) is the one standard deviation and is given in terms of the least unit cited (e.g., 0.0196 (30) represents 0.0196 ± 0.0030, and 20.4 (39) represents 20.4 ± 3.9). [a]Calculated for basalts and picrites compositions reported by Larsen and Pedersen (2009). [b]R_0 is calculated assuming 90% depleted MORB mantle (DMM) (Salters & Stracke, 2004) + 10% normal-MORB (N-MORB) (Gale et al., 2013).

All mineralogies that can satisfy Equation 2 for all five ratios are selected and are deemed the "passed" mineralogies. The best-fit mineralogies are those with the lowest BulkRes values.

3.2. Choice of the Elemental Ratios

In geochemical modeling, the most primitive samples (i.e., those with the highest MgO contents) are usually thought to best preserve the liquid compositions in equilibrium with the mantle. It is also generally accepted that, at low pressure (<1 GPa), basalts with more than 8 wt.% MgO have only fractionated olivine (Klein & Langmuir, 1987). Such fractionation effects are relatively easy to correct for (e.g., Herzberg & Asimow, 2015; Lee et al., 2009). However, higher pressure of fractionation can result in early crystallization of pyroxenes (e.g., Eason & Sinton, 2006) that can result in an erroneous evaluation of the parental melt composition (e.g., Herzberg & Asimow, 2015). Additionally, no basalts with more than 8 wt.% MgO were recovered at Sites U1571 or U1572 (Figure S1 in Supporting Information S1). Hence, it is crucial to evaluate the effect of fractionation on the ratios used in the model. In this section, we provide the reasoning behind the selection of the elemental ratios used in this model and explanations on why some ratios (e.g., Ni/Co, Co/Fe) previously used in the literature as a proxy for the presence of pyroxenite in the mantle source (e.g., Chen et al., 2022; Davis et al., 2013; Le Roux et al., 2011; Zhang et al., 2012) were not selected here.

The selected ratios were chosen so (a) they are not significantly affected by fractionation (see Appendix B). For instance, Ni/Co decreases rapidly during fractionation processes. Hence, the ratio observed in basalt is likely very different from the ratio of the primary magma, making Ni/Co a poor candidate for our model. (b) Different mantle mineralogy would produce contrasted melt ratios (see Appendix B). (c) As R_0 for each ratio is kept constant in our model (Equation 1), the ratio in the mantle source must be relatively independent of the mantle lithology (see Appendix C). For instance, Co/Fe is not a suitable candidate for our model because natural peridotites and pyroxenites show contrasted ratios that prevent us from choosing a unique R_0 value for the bulk mantle. We also eliminated V/Sc as this ratio is known to be particularly sensitive to changes in oxygen fugacity (e.g., Lee et al., 2005; Li & Lee, 2004). Finally, ratios involving Cu have been discarded because hydrothermal activity and seawater-basalt interaction can result in an increase of the copper content in the basalts (e.g., Dekov et al., 2013). Such metasomatic enrichments have been documented in tholeiites from ODP Site 642 on the Vøring Plateau (LeHurray, 1989). Using this strategy, the selected ratios for our models are Mn/Fe, Zn/Fe, Mn/Zn, Sc/Zn, and Ga/Sc (Table 1).

3.3. Choice of the Mantle Assemblage

A potential limitation of our model is the assumption of an anhydrous 5-phase (ol, opx, cpx, grt, sp) mantle source. These minerals were chosen as they likely represent the primary phases associated with main mantle lithologies, but we cannot rule out the presence of accessory minerals, such as sulfides (e.g., Usui et al., 2022), or hydrous minerals (e.g., Veter et al., 2017).

Sulfides found in mantle xenoliths are primarily composed of Fe with minor amounts of Ni and Cu (Kiseeva et al., 2017). Because of the highly compatible behavior of Ni and Cu in sulfides (Kiseeva & Wood, 2015), their partitioning behavior during mantle melting may be strongly affected by the presence of sulfide in the source despite the very low abundance of the latter (<<1% of the bulk rock). However, due to iron's presence as a major element of the bulk upper mantle, it is not significantly affected by the presence of such a small amount of sulfides in the source.

The presence of hydrous phases in the mantle source may also affect the partitioning behavior of some FRTEs. In fact, recent studies (e.g., Condamine et al., 2022; Ezad et al., 2025; Foley et al., 2025) have shown that hydrous minerals exert strong control on several first-row transition elements. For the elements considered in this study, partition coefficient data between basaltic melt and hydrous phases are scarce. Recent experimental results from Ezad et al. (2025) between phlogopite and lamproite and between amphibole and basanite suggest that the behavior of FRTEs within these minerals is relatively similar to olivine, except for Sc, which seems to be compatible in amphibole (we note that the experimental partition coefficient for Sc between amphibole and basanite varies from 0.94 to 9.69). Hence, if residual phlogopite is present in the mantle source, it may result in an overestimation of the olivine mode.

Alternatively, if amphibole is present in the mantle source, this might result in an overestimation of olivine and garnet. However, when present in the mantle source, hydrous phases are usually the first phases to be exhausted during magma genesis (e.g., Médard et al., 2006; Rosenthal et al., 2009). In addition, amphibole- or phlogopite-bearing assemblages tend to produce strongly silica undersaturated alkali basalts (Pilet, 2015; Pilet et al., 2008). The subalkaline nature of the basalts collected on the Vøring Margin does not support the presence of residual hydrous phases in their mantle source.

3.4. Calculated Mantle Mineralogy

In the section below, we describe the outputs of our model for each site, which are plotted in Figures 4 and 5. Additional projections to visualize changes in garnet and clinopyroxene independently are presented in Figure S2 in Supporting Information S1. Calculations were performed with the R_B, R_0 and their associated one standard deviation listed in Table 1 (see also Appendix C), with a constant $F = 0.08$ (see Appendix B) and $n = 10{,}000{,}000$. Table 2 presents the average best-fit mineralogy and its one standard deviation for each site.

Calculated passed mineralogies present significant overlap between the sites (Figure 4 and Figure S3 in Supporting Information S1). This is not surprising considering the overlap of the average element ratios and their associated standard deviations used in this model (Figure 2). Part of the scatter can also be explained by the behaviors of the exchange coefficients for the considered elements, as the relative order of the exchange coefficients between the five minerals is the same for the five element ratios considered in this model, making decoupling the signal for these minerals more challenging.

Despite this large overlap, a number of observations can be made: (a) Overall, passed mineralogies at Site U1566 are richer in olivine (and spinel), and passed mineralogies for basalts at Site U1571/72 are richer in clinopyroxene (and garnet) in comparison to the other sites. Through conducting pairwise MANOVA (multivariate analysis of variance) tests, we found that the differences in output mineralogy from all sites were statistically significant (p-value << 0.05). (b) The proportion of garnet never exceeds 10% (Figure S2 in Supporting Information S1). (c) Site U1573 shows output mineralogy distribution intermediate between U1566 and U1571-U1572. (d) The proportion of outputs for Site U1574 is significantly lower than for the other sites, and the source mineralogy at this site stands out for its very low fraction of garnet (only 30% of outputs present garnet fraction equal or higher than 1%) and higher proportion of orthopyroxene than at the other sites.

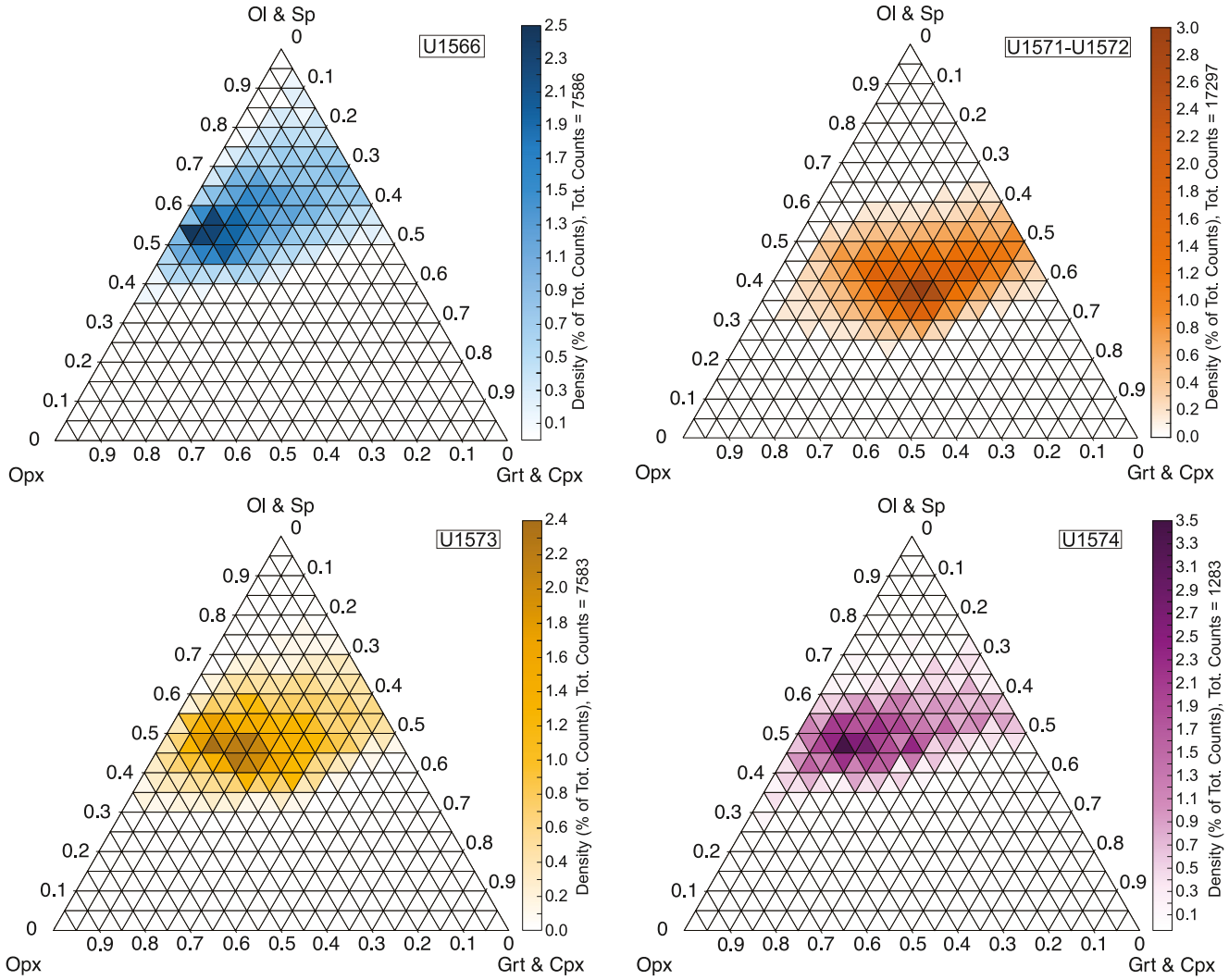

Figure 4. Vøring Margin source mineralogies by site. Ternary density plot showing the source mineralogies that satisfy constraints on the combined five ratios (i.e., the passed mineralogies) in the ternary diagram Olivine + Spinel – Garnet + Clinopyroxene – Orthopyroxene (scatter plots of the all passed mineralogies are depicted in Figure S3 in Supporting Information S1). The run was conducted with $n = 10{,}000{,}000$ and mode constraints as Xol = 0 to 1, Xcpx = 0 to 1, Xopx = 0 to 0.9, Xgrt = 0 to 0.3 and Xsp = 0 to 0.1. Total numbers of passed mineralogies are 7,586 for Site U1566, 17,297 for Sites U1571-U1572, 7,583 for Site U1573, and 1,283 for Site U1574. Color scales indicate density as a percent of total number of outputs.

4. Discussion

4.1. Mantle Potential Temperature During the Northeast Atlantic Breakup

The association of the North Atlantic volcanic rifted margins with the Iceland hotspot (e.g., Bijwaard & Spakman, 1999; Montelli et al., 2004; Ritsema et al., 1999) has led to the hypothesis that high magmatic productivity may have resulted from high temperatures caused by a mantle plume (e.g., McKenzie & Bickle, 1988; White & McKenzie, 1989). In fact, published T_P estimates for Paleocene lavas of the NAIP are up to 1610°C (e.g., Hole & Millett, 2016; Larsen & Pedersen, 2000, 2009; Spice et al., 2016; Willhite et al., 2019). However, most previous T_P assessments for the NAIP have been performed using picritic samples. The bulk composition of the picrites is corrected for olivine accumulation to obtain the primary magma composition. Olivine grains in picrite are not in equilibrium with the magma, so such correction usually results in overestimation of the required potential temperatures (Borchardt & Lee, 2022; Hole & Natland, 2020; Shellnutt & Pham, 2018).

Using aphyric lavas that have only crystallized olivine, Hole and Natland (2020) obtained a maximum temperature of ~1500°C for Baffin Island and Disko Island, suggesting that many existing T_P estimates are

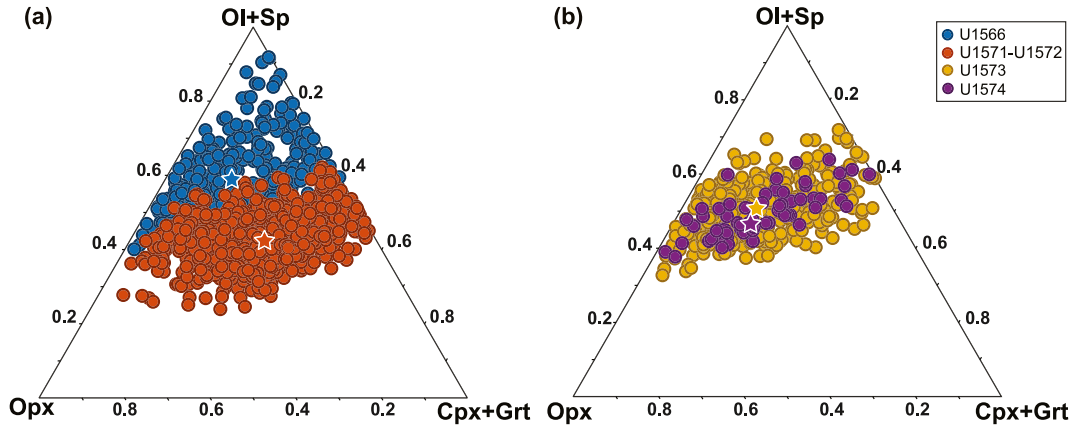

Figure 5. Best-fit source mineralogies. The 5% best-fit for the passed mineralogies presented in Figure 4. Sites U1566 and U1571-U1572 are plotted in ternary (a), while Sites U1573 and U1574 are plotted in ternary (b) for legibility. Star symbols represent the average calculated mineralogy for each site.

overestimated. Using the same criteria, we obtained similar temperatures for both East and West Greenland and for the Vøring margin (see Text S2 and Figure S4 in Supporting Information S1 for details). With the inherent uncertainty of the model being ±40°C (Herzberg & Asimow, 2015), our results suggest that lava flows emplaced on West and East Greenland 61 Ma and on the Vøring Margin ~56–50 Ma, coinciding with the two main phase of magmatism during the emplacement of the NAIP (Jones et al., 2023; Storey, Duncan, & Tegner, 2007; Wilkinson et al., 2017 and references therein), record similar mantle T_P.

It is also important to highlight that calculated T_P are highly dependent on the chosen Mg# (=Mg/(Mg + Fe_t), in mol.%) of the source. Our calculations were performed with an Mg# expected for a garnet peridotite (Mg# = 0.916; Walter, 1998). Decreasing the Mg# would result in a decrease of the forsterite content for the olivine in equilibrium with the source and in a decrease of the estimated T_p. Borchardt and Lee (2022) suggested that the possible maximum olivine forsterite content in equilibrium with NAIP magmas is 90.9. For such Fo content, the calculated average T_P for the NAIP is as low as 1420°C. The average Mg# for natural peridotites and pyroxenites are 0.92 ± 0.02 (1σ) and 0.82 ± 0.10 (1σ) (see Appendix B). Hence, the presence of pyroxenitic lithologies in the source is expected to decrease the bulk Mg# of the source and the mantle potential temperature required to explain the basalt compositions. Adding volatiles in the source would have a similar effect. Using Lee et al.'s thermobarometer (2009), we estimate that adding 1 wt.% H_2O in the parental melt results in a decrease of the calculated T_P of 20–30°C. Hence, in the following discussion, we consider T_P = 1500°C as a maximal value for the emplacement of the NAIP.

Table 2
Best-Fit Source Mineral Assemblages

	U1566	U1571-U1572	U1573	U1574	West Greenland[a]
Olivine	56.0 ± 9.1	41.8 ± 6.2	49.2 ± 7.0	46.0 ± 5.4	44.1 ± 8.2
Clinopyroxene	14.2 ± 8.9	28.6 ± 11.6	16.1 ± 9.7	16.3 ± 9.3	25.4 ± 12.2
Orthopyroxene	25.1 ± 13.3	26.6 ± 13.4	31.6 ± 12.9	35.4 ± 12.0	26.0 ± 12.9
Garnet	1.63 ± 1.2	2.02 ± 1.3	1.38 ± 1.1	0.52 ± 0.4	3.09 ± 2.0
Spinel	3.12 ± 1.0	0.95 ± 0.6	1.69 ± 0.6	1.80 ± 0.6	1.39 ± 0.9

Note. Average of the 5% best-fit mineralogy (in %) and one standard deviation calculated at each site. Average and standard deviation calculated on all passed mineralogy are presented in Table S5. [a]Calculated on picrite and basalt from West Greenland reported by Larsen and Pedersen (2009) for the same number of best-fit mineralogies reported by U1571-U1572.

4.2. Implications for the Formation of the Vøring Margin

4.2.1. Role of Lithospheric Thinning

Meyer et al. (2009) suggested that lithospheric thinning may play an important role in the opening of the Northern Atlantic. In their model, the lithosphere was substantially thinned during rifting periods prior to the breakup (Wangen et al., 2008), promoting mantle upwelling and the production of melt. These melts then underplate the crust, eventually inducing crustal anatexis (e.g., Morris et al., 2024). Finally, these crustal melting processes weaken the crust in such a way that further rifting results in the final breakup and the emplacement of thick packages of lava visible as Seaward Dipping Reflectors (SDR).

Using Melt-PX (Lambart et al., 2016), we can estimate the effect of lithospheric thinning by calculating the crustal thickness generated by a peridotitic mantle with and without a lithospheric lid. We performed calculations at $T_P = 1500$°C, using a lithospheric thickness of 60 km, that is, the thickness estimated for the Vøring plateau at the transition to the oceanic domain (Fernández et al., 2004). The density of the lithosphere and of the generated mafic crust are set up to 3,300 and 3,000 kg m^{-3}, respectively. The generated thickness of basaltic crust increases from 6 km when melting stops at the base of the lithosphere, to 21 km when melting continues up to the base of the crust, consistent with the estimation for the mafic crustal thickness observed near the continent-ocean transition (Mjelde et al., 2005). Such results would point toward a rapid rupture of the mantle lithosphere rather than a progressive thermal erosion (e.g., Brune et al., 2016).

Rapid rupture of the lithosphere is supported by Lu and Huismans (2021), who produced numerical models showing that a rupture of the lithospheric mantle before the crust can result in enhanced magmatic production in the distal margin. The authors suggested such a scenario would require a modest thermal anomaly ($\Delta T < 100$°C) to explain the excess magmatism observed in continental margins such as the NAIP. Significant stretching of the crust before the local peak of magmatic activity is also supported by the presence of a peraluminous dacitic flow unit between the lower and the upper series in ODP Hole 642E (Viereck et al., 1988). This dacitic unit is thought to have the same origin as the dacite flow recovered during IODP Expedition 396 in early Eocene sediments in the Vøring Basin (Site U1570; Planke et al., 2023a), which has been interpreted as the result of upper crustal anatexis at low pressure (<5 kbar) at 54.6 ± 1.1 Ma (Morris et al., 2024).

However, the rapid rupture of the lithosphere alone cannot explain the results of our Monte Carlo simulations. Basalts collected from Site U1566 record the most refractory source mineralogy of all Exp. 396 lavas (Table 2); they were emplaced in the latest Paleocene and are thought to represent the earliest rift magmatism on the Vøring Margin. In comparison, the best-fit mineralogies of basalts at Sites U1571-U1572, which represent the top of the SDR sequence, are significantly richer in clinopyroxene (Figures 4 and 5; Planke et al., 2023c). At Site U1573, which is thought to represent the transition to a more mature oceanic crust (Planke et al., 2023e), the best-fit mineralogies are more similar to those at Site U1566, though they contain less olivine, slightly less spinel, and are richer in orthopyroxene. The contrast between each site implies that the proportion of minerals that contribute to the melting reactions changed with time. In particular, the contribution of clinopyroxene is more elevated during the peak of magmatism.

In addition to the presence of SDR, volcanic rifted margins are characterized by the presence of high P-wave velocity Lower Crustal Bodies (LCBs). The mid-Norwegian Margin is no exception, as these LCBs have been identified in both the proximal and distal parts of the margin. While the proximal LCBs are interpreted by some authors as inherited, high-pressure granulite/eclogite lower crustal rocks (e.g., Gernigon et al., 2006; Nirrengarten et al., 2014), distal LCBs are usually interpreted as underplated magmatic cumulates at the base of the crust (e.g., Berndt et al., 2001; Eldholm et al., 1989; Larsen & Saunders, 1998; Mjelde et al., 2005; Planke et al., 2005; Talwani & Eldholm, 1977). Underplated material in distal LCBs is considered to be part of the excess magma produced during the emplacement of large igneous provinces and is usually thought to be formed before or during the emplacement of the SDR (e.g., Lu & Huismans, 2021; Meyer et al., 2009). In such a scenario, the magma that formed the upper SDR must then have interacted with underplated material on its way to the surface, as suggested by the lower series of the Hole 642E samples (Meyer et al., 2009) and Site 917 from Southeast Greenland coast (Fitton et al., 2000).

Another important aspect of our results is that the apparent source of SDR at Site U1571-U1572 may be slightly richer in garnet than the source of magma at Site U1566. While the variations between the two sites are small

(Table 2), they appear contradictory with a thinning of the lithosphere that should result in a decrease of the average melting pressure.

Recently, Rooney et al. (2023) proposed that melting of the metasomatized subcontinental lithospheric mantle may play a role in the generation of the Afar Stratoid Series in East Africa. In line with this conceptual model, we hypothesize that mantle-derived magma during the initiation of rifting on the Vøring Margin must have percolated through a thick continental lithosphere, where in situ crystallization along the way to the surface may have contributed to the production of metasomatic veins in the continental mantle lithosphere and of underplated material at the base of the crust (Figure 6). As the lithosphere is further stretched and thinned during rifting, the geotherm adjusts to a thinner lithosphere, resulting in a remobilization of the metasomes and underplated material.

To test this model, we used alphaMELTS (software: Smith & Asimow, 2005; thermodynamic models: Ghiorso & Sack, 1995; Asimow & Ghiorso, 1998) to estimate the mineralogy of magmatic cumulates produced by a melt representative of the primary magma at Site U1566 at 7 kbar (i.e., Moho depth) and at 19 kbar (i.e., base of the lithosphere) (see Text S3 in Supporting Information S1 for additional details). Assuming that the primary magma is anhydrous, the calculated underplated material is composed of olivine, pyroxenes, and feldspars (in proportion 0.1:0.6:0.2, while the metasomatic veins are dominated by garnet and clinopyroxene (in proportion 0.3:0.6; Table S4).

As mentioned above, we cannot rule out that the metasomatic melts might be hydrated. Such melts will likely result in crystallization of amphibole-bearing metasomes. Hence, the apparent slight increase in the garnet mode may actually reflect an increase in amphibole in the source. Without better constraints on the partitioning behavior of FRTEs and Ga between amphibole and basaltic melt, distinguishing between each scenario becomes challenging. The slight negative slope in heavy rare earth elements only observed for basalts are Sites U1571-U1572 is however consistent with the presence of small fraction of residual garnet in their source (Figure S5 in Supporting Information S1). Coupled with Lu and Huismans (2021)'s scenario, a similar model could explain both the excess of magmatic productivity associated with the emplacement of the SDR and the evolution of the source mineralogy during break-up (Figure 6): during the initiation of rifting (Site U1566), thinning of the plate facilitates upwelling of the underlying upper mantle, causing decompression melting. Melt produced during this period must have traveled through a relatively thick lithospheric mantle and continental crust, resulting in crustal contamination (Figure S6 in Supporting Information S1). We note that a large amount of crustal assimilation may result in a change of basalt composition. However, crustal contamination alone cannot explain the difference between Sites U1566 and U1571-U1572, as such processes will result in opposite trends for the elemental ratios used in the model (Figure S7 in Supporting Information S1).

During their transport to the surface, melts that do not reach the surface may accumulate at the Moho and form gabbroic underplated material or may crystallize in the lithospheric mantle and form clinopyroxene-rich metasomes. As stretching of the lithosphere continues, thermal re-equilibration of the lithosphere results in crossing the solidus of the metasomes and the underplated material. By mixing with the magma produced by the melting of the plume-influenced asthenospheric mantle, the additional contribution of this mafic material would result in an apparent increase of pyroxene and garnet in the mantle source, consistent with our observations at Site U1571-U1572. As rifting progresses through the development of a more mature oceanic crust, the lithosphere is now thermally re-equilibrated, and the magma source progressively returns to a decompression melting of the asthenospheric mantle, consistent with lavas at Site U1573 showing apparent mineralogy intermediate between Site U1566 and Site U1571-U1572.

4.2.2. Role of the Mantle Plume

The contribution of plume material is required to explain some of the compositional features common between magmas emplaced during the formation of the NAIP. For example, basalts in the region present high $^{3}He/^{4}He$ and/or radiogenic Sr-Nd-Pb signatures (e.g., Brown & Lesher, 2014; Hole & Natland, 2020; Koptev & Cloetingh, 2024; Stuart et al., 2003; Tegner et al., 1998). However, the shift of source mineralogy calculated in our study is harder to explain solely by the contribution of plume material. The basalts at Site U1566 record an average mineralogy of a typical mantle peridotite (Table 2). Assuming that average source mineralogy at Site U1571-U1572 reflects a mix between peridotite and olivine-free pyroxenite, this would correspond to ∼25% fraction of pyroxenite. Because of the high density of pyroxenite compared to peridotite, to preserve mantle

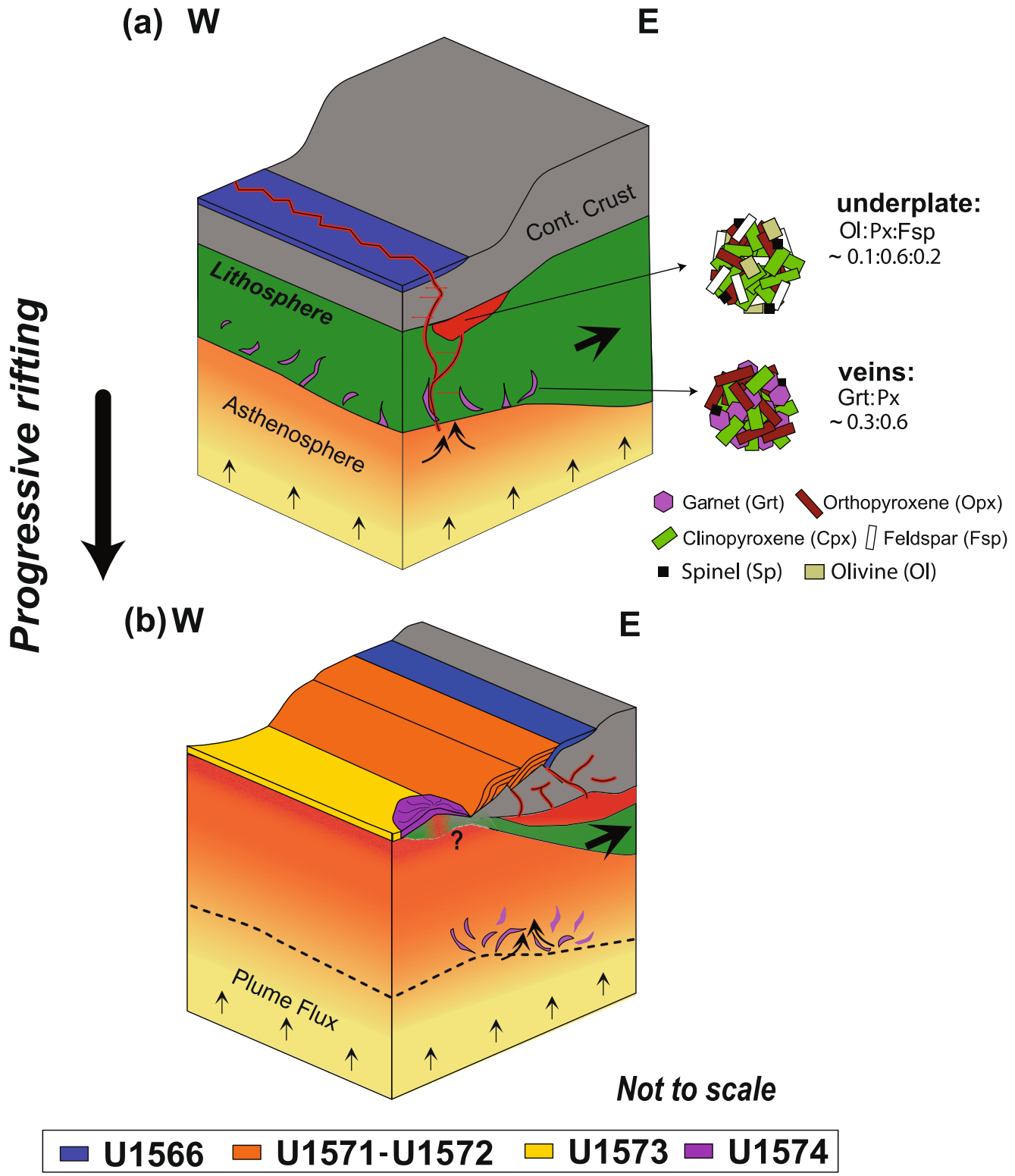

Figure 6. Cartoon illustrating the role of the subcontinental lithosphere during rifting and the formation of the Vøring margin. (a) Block diagram illustrating the initiation of rifting (Site U1566) and formation of lithospheric veins and magmatic underplate. Mineral relative proportions for the underplate and veins were calculated using alphaMELTS (Smith & Asimow, 2005) at 7 kbar (Moho depth) and 19 kbar (lithospheric depth), respectively. (b) Block diagram illustrating magmatic processes as lithospheric stretching continues: the veins and the underplated material are remobilized during the emplacement of the SDR (Sites U5171-U1572). At the COB, basalts record a higher degree of interaction with the continental lithosphere (Site U1574; see Section 4.3 for details). As the thermal gradient progressively re-equilibrates the main source of magma transitions back to the asthenospheric mantle (Site U1573).

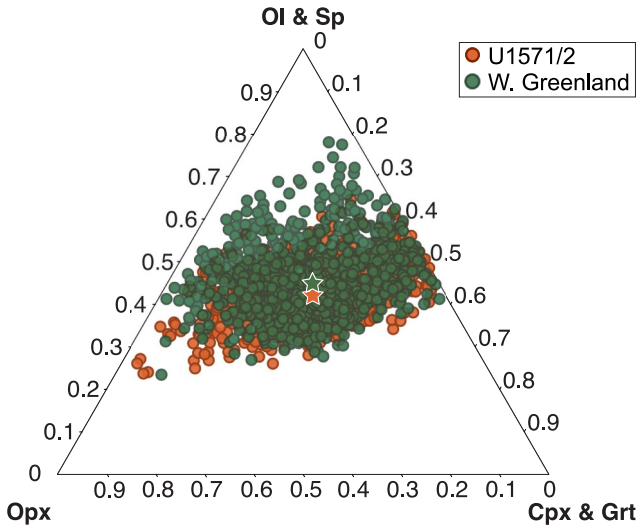

Figure 7. Source mineralogy comparison between Sites U1571-U1572 and West Greenland. Ternary density plot obtained for all passed mineralogies using basalt and picrites compositions reported by Larsen and Pedersen (2009) compared with the density plot obtained for site U1571-U1572. See Figure S8 in Supporting Information S1 for scatter plot comparison of the best-fit mineralogies.

buoyancy, increasing the fraction of pyroxenite in the source also requires a significant increase the mantle potential temperature (Brown & Lesher, 2014) or must be compensated by the presence of a third light mantle lithology, such as refractory harzburgite (e.g., Shorttle et al., 2014; Stracke & Béguelin, 2024). As a comparison, for $\Delta T_P \leq 150$°C, Brown and Lesher (2014) calculated that the maximal fraction of pyroxenite that can be present in a mantle plume composed of pyroxenite and peridotite is ~15%. Above this, the mantle plume is not buoyant (see also Text S4 in Supporting Information S1).

Interestingly, best-fit mineralogies obtained at Site 1571-U1572 almost fully overlap with best-fit mineralogy calculated for the source of the Paleocene lavas from West Greenland (Figure S8 in Supporting Information S1; Larsen & Pedersen, 2009). Compositions reported by Larsen and Pedersen (2009) (Table 1) result in a larger scatter in the passed mineralogies, but the density plots (Figure 7) for the two locations also coincide. Multiple pieces of evidence suggest that the magmatic activity has fluctuated (or pulsed) during (e.g., Hartley et al., 2011; Millet et al., 2020; Mjelde & Faleide, 2009; Saunders et al., 1997) and after (e.g., Parnell-Turner et al., 2014; Spice et al., 2016) the emplacement of the NAIP. Koptev and Cloetingh (2024) recently suggested that the West Greenland magmatism resulted from the remobilization of "dormant" plume material accumulated at the lithosphere asthenosphere boundary during its path from West to East Greenland between 90 and 60 Ma (Steinberger et al., 2019). In their model, spreading axis propagation from the Labrador Sea toward Baffin Bay resulted in lithospheric thinning and remobilization of this plume material. For the basalts emplaced on the Vøring margin, an accumulation of plume material before the initiation of rifting is unlikely, as the basalts collected at Site U1566 record a relatively refractory source mineralogy (Figure 4, Table 2). However, both studies highlight the importance of refertilization of the lithosphere and strong lithospheric thinning associated with the peak of magmatic activity. Hence, we propose that the lithosphere refertilization that occurred during the initiation of rifting might be an essential component of the NAIP widespread magmatism.

Koptev and Cloetingh (2024) proposed a new classification for LIPs with two main categories associated with continental breakup: "LIP producer," where the presence of the mantle plume is directly responsible for the location and timing of continental breakup, and "LIP trigger" for which the magmatic activity associated with the LIP is preceded by continental rifting. Our model is consistent with the LIP trigger phenomenon, for which the role of the plume in the peak of magmatic activity is to enhance the ongoing localized extension related to pre-magmatic rifting. The main driver of the rapid increase of magmatic flux is the rifting process itself and the rupture of the mantle lithosphere.

4.3. Nature of the Outer High (Site U1574)

At Site U1574, Expedition 396 sampled Eldhø, an Outer High on the Vøring Margin. Eldhø has been interpreted as an extinct volcano, formed by shallow, emergent marine volcanism near the continent-ocean boundary (Planke, Berndt, Alvarez Zarikian, Bünz, et al., 2023). In comparison to the other sites, the source mineralogy calculated for Site U1574 shows an orthopyroxene-enrichment and very low fraction of garnet (Table 2). The mantle potential temperature calculated for Site U1574 is 1480°C (Figure S4 in Supporting Information S1), the only site from Expedition 396 that produced a result from PRIMELT3 without an associated warning, suggesting that the thermal anomaly was still present during the emplacement of the basalts at this Site. Palynology indicates that basalts collected at Sites U1571-U1572, U1573, and U1574 were all emplaced in the late Early Eocene (Planke et al., 2023c, 2023d, 2023e).

Surprisingly, basalts recovered at Site U1574 show low Nb/U and Ce/Pb ratios (Figure S6 in Supporting Information S1), similar to the ratios observed for basalts at Site U1566. Such low ratios are often interpreted as a signal for crustal contamination (Hofmann et al., 1986). Available geophysical data do not necessarily support the presence of crustal material beneath Eldhø: gravity data do not show any evidence for light crustal material at depth, and Inner SDR are dipping toward Eldhø, suggesting significant subsidence (Planke et al., 2023e).

However, crustal fragmentation has been previously invoked on the Vøring Plateau, for instance, to explain the presence of two sequences of Inner SDR (Berndt et al., 2001), and we cannot rule out that the current data cannot resolve such small length scale variations. Additionally, previous studies support the presence of continental fragments within ocean basins in multiple locations, including beneath Jan Mayen and Iceland (Torsvik et al., 2015; Niu, 2025, and references therein).

Alternatively, low Nb/U and Ce/Pb ratios may reflect the signature of an old lithosphere infiltrated by silicate melts, with ratios consistent with global subducted sediment (i.e., GLOSS; Plank & Langmuir, 1998). In fact, the relatively high MgO contents of the basalts at Site U1574 (Figure S1 in Supporting Information S1) argue against a high degree of crustal assimilation. The orthopyroxene-enrichment at Site U1574 supports the effect of melt interaction with the lithosphere (e.g., Jing et al., 2019; Pin et al., 2022). In addition, both the calculated low fraction of garnet (Table 2) and the high SiO_2 content of the basalts at Site U1574 support a process happening at low pressure (Figure S9 in Supporting Information S1; van den Bleeken et al., 2011). Finally, the multiple subduction episodes during the Scandinavian Caledonides evolution ∼400–500 Ma (e.g., Brueckner & van Roermund, 2004) could have resulted in the lithosphere beneath the Vøring Plateau at the time of rifting to present signatures of an ancient metasomatized subcontinental lithospheric mantle.

Outer Highs are common volcanic seismic facies associated with rifted margins, usually located at the boundary between the continental and the oceanic domains (Planke et al., 2000). With or without the presence of crustal material, a high degree of interaction with the continental lithosphere may record a local decrease of magmatic activity and slower magma ascent rates. In comparison, at Sites U1571-U1572, only the top of the Inner SDR sequence was sampled. By the time these basalts were emplaced, active upwelling and previous magmatic activity may have facilitated rapid melt extraction without significant interaction with the continental lithosphere.

Work beyond the scope of this study is required to confirm this working hypothesis, including (a) precise assessment of the age of the basaltic basement at each drilling site. Our current hypothesis is consistent with the preliminary ages obtained from palynology (Planke et al., 2023d), suggesting that the Outer High and basalts at Sites U1571-U1572 and U1573 were emplaced in the Early Eocene, but refinement of these ages may help in supporting our hypothesis. (b) Sampling of other Outer Highs at volcanic margins and comparing observations would help to assess if Eldhø is representative of all Outer Highs at volcanic rifted margins.

5. Conclusions

We used the geochemistry of basaltic samples collected from the mid-Norwegian Margin during International Ocean Discovery Program Expedition 396 to evaluate the driving mechanisms of excess magmatism associated with the break-up of Greenland and Eurasia. Basalts used in our study represent five sites drilled during the expedition, ranging from the initiation of rifting to the peak of magmatism, and ending with the transition to a marine environment. Using a Monte Carlo statistical approach based on elemental ratios (Mn/Fe, Zn/Fe, Mn/Zn, Sc/Zn, and Ga/Sc) of the basalts, we demonstrate that the mantle source saw a change of mineralogy on a short timescale (a few million years) with a clinopyroxene enrichment coinciding with the peak of magmatism.

We propose a geodynamic model where both the presence of a mantle plume and substantial thinning of the lithosphere are required. We proposed a scenario in three steps where (a) the initiation of rifting results in the melts derived from a mantle-plume influenced asthenosphere to travel through a thick lithosphere. These melts either reach the surface after suffering from crustal contamination or are trapped in the lithospheric mantle or at the Moho (underplated material). (b) Further stretching of the lithosphere results in remobilization of this mafic material and finally leads to the rupture of the mantle lithosphere, allowing for additional magmatic productivity. (c) While rifting continues, the geotherm re-equilibrates and magmas once again mostly sample a plume-influenced asthenospheric mantle source.

Appendix A: Bulk Composition Analyses

Bulk rock major element analyses were done using the Thermo Scientific ARL X-ray fluorescence (XRF) spectrometer at the Institute of Geochemistry, Chinese Academy of Sciences. BHVO-2 and BCR-2 were used as secondary standards. For the same samples, bulk rock trace element concentrations were analyzed using Agilent-7900 inductively coupled plasma mass spectrometer (ICP-MS) at the Institute of Oceanography, Chinese Academy of Sciences, following procedures of Chen et al. (2017). In brief, ∼50 mg of each sample was dissolved

with an acid mix of double-distilled concentrated HCl + HNO_3 and HF in a high-pressure bomb for 15 hr and then re-dissolved with distilled 20% HNO_3 for 2 hr until complete digestion/dissolution of the sample. BHVO-2 was used as a secondary standard. Analytical accuracy is better than 5% for all major elements and Sc, Ni, Co, Ga, Nb, U, Ce, and Pb. Analytical accuracy is between 5% and 10% for Cr, Mn, and Cu, and better than 15% for Ti, V, and Zn (Tegner et al., 2025).

A secondary set of samples was analyzed for trace element concentrations at Niigata University (Japan) using a Yokogawa HP4500 ICP-MS, following the acid digestion method described in Senda et al. (2014). For each sample, 100 mg of material was weighed and placed in a Teflon vial, and underwent step-by-step acid treatment with heating until the sample reached complete dissolution. The solution was finally diluted using HNO_3 and an internal standard (^{115}In) and was measured along with secondary standards (BHVO-2, W2a, and JB2). Analytical accuracy on secondary standards is better than 5% for all elements but Sc, Ga, Nb, and Pb. For these four elements, the analytical uncertainty is better than 10% (Tegner et al., 2025).

Finally, compositions obtained offshore during the expedition with ICP-AES are also reported in Table S1 and used to calculate the average elemental ratios (Table 1). A problem of calibration on SiO_2 during the expedition (see Planke et al., 2023f for details) prevents us from relying on the ICP-AES SiO_2 concentrations. However, for the other major elements, the good correspondence between ICP-AES and the XRF analyses performed in this study supports that compositions obtained from both techniques can be used to assess the compositional variability at each site. The excellent consistency with the portable-XRF analyses collected during the cruise for FeO, TiO_2, MnO, Ni, Zn, Cu, Sr, and Y also supports this choice (1–see also Planke et al., 2023b, 2023c, 2023e for details).

Appendix B: Effect of Fractionation and Alteration Processes

Ideally, the elemental ratios used in the model should stay constant during melting and fractional crystallization, and contrasted source mineralogy should result in contrasted elemental ratios. To test the effect of crystallization, we calculated the evolution of the composition of the melt during fractionation of olivine only and olivine and clinopyroxene using a 1:1 ratio (Figure B1). For the effect of melting (Figure B2), we followed the same approach as Lang and Lambart (2022), using the subsolidus modal proportion of the peridotite KR4003 at 3 GPa (Walter, 1998), and the near-solidus modal proportion of the MORB-type eclogite G2 at 3 GPa (Pertermann & Hirschmann, 2003). In all calculations, we used the set of partition coefficients presented in Table S2.

The ratios Ni/Sc, Ni/Co, and, to a lesser extent, Co/Fe rapidly drop during fractional crystallization (Figure B1). When clinopyroxene is also crystallizing, Ti/Cr shows the opposite evolution. Because for such ratios, the erupted

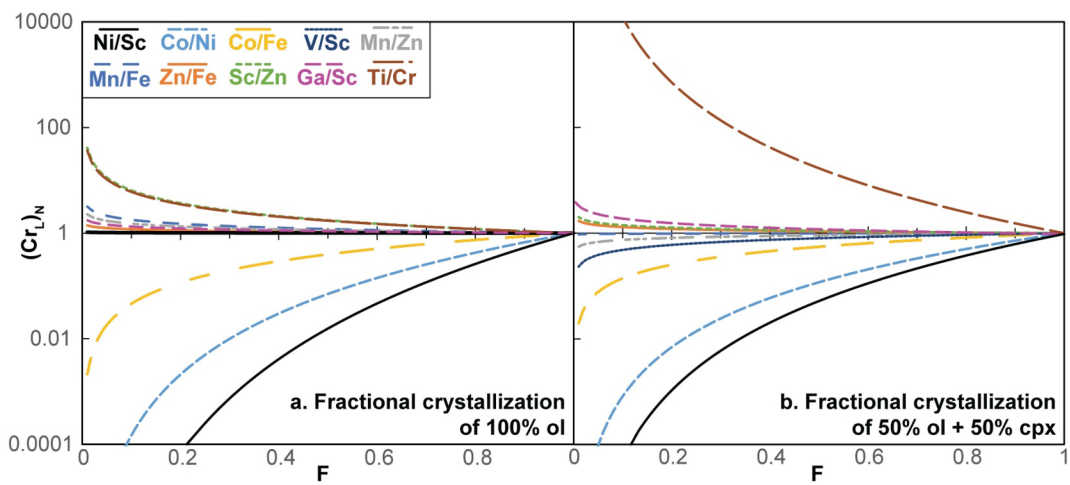

Figure B1. Normalized concentration ratios in liquid $(R_L)_N$ as a function of the melt fraction present in the system during fractional crystallization. Panel (a) considers fractionation of olivine only, and panel (b) considers fractionation of equal parts clinopyroxene and olivine. The partition coefficients for olivine and clinopyroxene used in the calculations are listed in Table S2 (Davis et al., 2013).

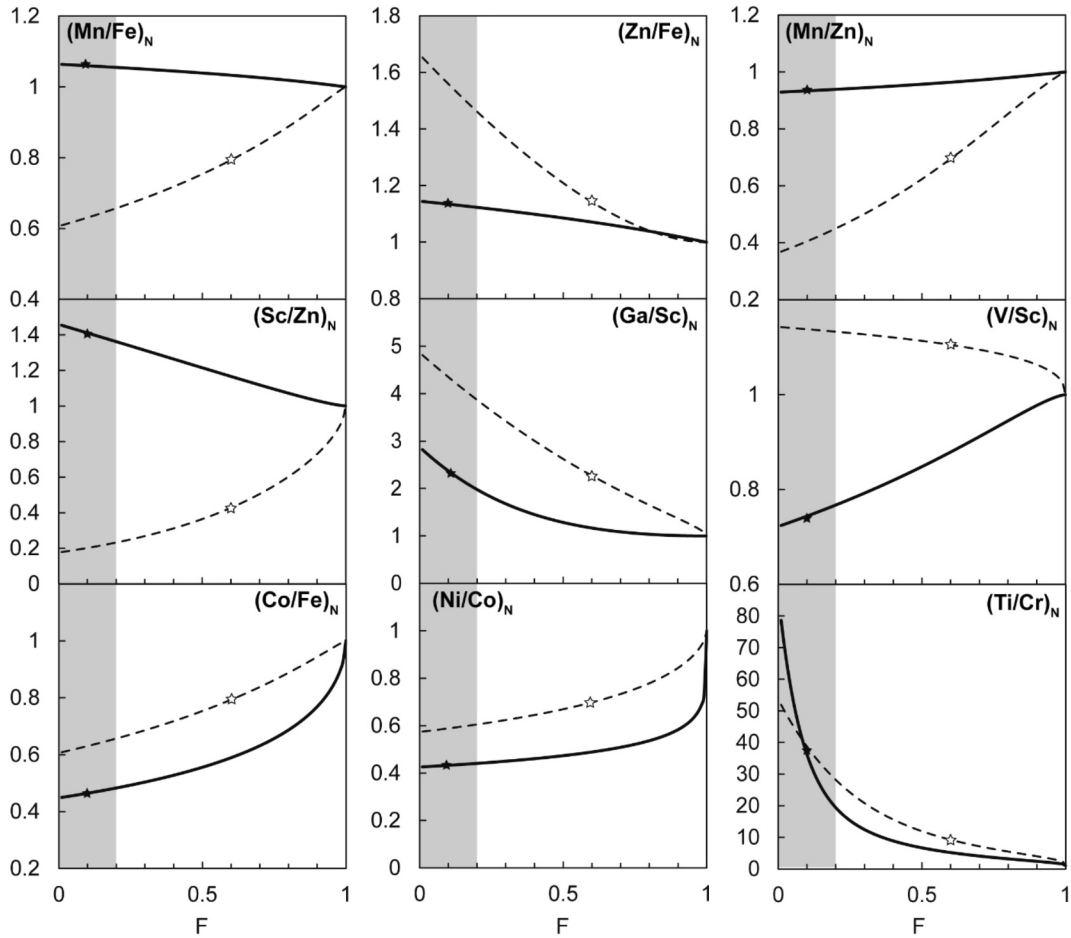

Figure B2. Evolution of the normalized elemental ratios with increasing melt fraction. Calculations done using the aggregated fractional melting equation (Equation 2) for two contrasted lithologies assuming the same source ratio R_0: a fertile peridotite (KG4003: 0.531 ol + 0.273 opx + 0.177 cpx + 0.019 grt, solid line; Walter, 1998) and a MORB-like type eclogite (G2: 0.82 cpx + 0.18 grt, dashed line; Pertermann & Hirschmann, 2003). The solid and open stars mark the value of the ratio at $F = 0.6$ for G2 and $F = 0.1$ for KG4003, respectively. Partition coefficients used in calculations are listed in Table S2.

basalts are unlikely to represent the ratios in the primary basalts, these ratios have been excluded from calculations. All the other ratios shown in Figure B1 present relatively low to moderate evolutions down to $F = 0.5$.

During melting, for $F \leq 0.2$, the lithologies that produced contrasted ratios are considered good candidates for tracing the bulk mineralogy of the source using primary magma compositions (Figure B2). Among the ratios tested here, only Ti/Cr did not fit these criteria. In the traditional approach of considering the presence of two separate lithologies, most pyroxenites are expected to achieve a higher degree of melting than peridotites (e.g., Hirschmann & Stolper, 1996). While most ratios still present contrasted values even when a higher degree of melting is considered for the pyroxenite lithology, the contrast in Ga/Sc and Zn/Fe ratios for the melt produced between the two lithologies decreases to the point that the ratios show no difference between peridotite and pyroxenite-derived melt. Hence, such ratios, as pointed out by Davis et al. (2013), may not be great candidates for solving for the proportion of pyroxenite in the source. In our approach, however, since we are not solving for the fraction of pyroxenite but for the bulk mineralogy of the source, we still consider these ratios to be good candidates to use in our model.

Finally, to test if the model is sensitive to moderate degrees of alteration, we also ran our calculations considering only basalts with LOI < 3 wt.% (and MgO > 5 wt.%). We found that the output density plots show slight differences between the two data sets (Figure S10 in Supporting Information S1 and Table S8), but the overall distribution and interpretation of the results are unchanged.

Appendix C: R_0 Values

Utilization of the aggregated fractional and batch melting equations requires the assumption of an initial source composition (R_0; Table 1). We downloaded natural pyroxenite and peridotite bulk compositions from the Interdisciplinary Earth Data Alliance (IEDA)'s EarthChem-PetDB online database. For pyroxenites, we considered analyses from pyroxenites, clinopyroxenites, orthopyroxenites, eclogites, and websterites. For peridotites, analyses from dunites, wehrlites, harzburgites, and lherzolites were selected. Samples are from alpine massifs, ophiolites, and mantle xenoliths. Samples with major element totals less than 90 wt.% and/or LOIs higher than 10 wt.% were systematically removed before any additional filtering. Compositions with more than three major element oxides falling outside of the initial three standard deviation envelope calculated on each data set were also excluded. The same filtering process was applied for elements considered in this study (FRTEs + Ga). For all selected ratios, the middle ranges for both lithologies overlap (Figure C1). On the contrary, ratios such as Co/Fe, Ni/Co, or Ni/Sc present contrasted values between each lithological group. Hence, we considered them as bad candidates in our model that uses a constant R_0 value. In our calculations, we used the ratio corresponding to a mantle composed of 90% DMM (Salters & Stracke, 2004) and 10% N-MORB (Gale et al., 2013). The R_0 values and their one standard deviation (Table 1) are also plotted on Figure C1 for comparison.

We also tested our model using R_0 values corresponding to a mantle made of pure DMM (Salters & Stracke, 2004). This test resulted in a lower number of outputs, supporting the assumption of a slightly more fertile mantle source for the NAIP, but the distributions of passed mineralogies are very similar between the two tests (Figures S11 and S12 in Supporting Information S1; Table S6).

Finally, we conducted a test that accounts for the uncertainty of partition coefficients (Table S2). The mineralogy distributions at each site show slightly more scatter (Figures S13 and S14 in Supporting Information S1; Table S7), and the number of outputs is similar or slightly lower than for calculations run with constant D values, but the general trends are the same.

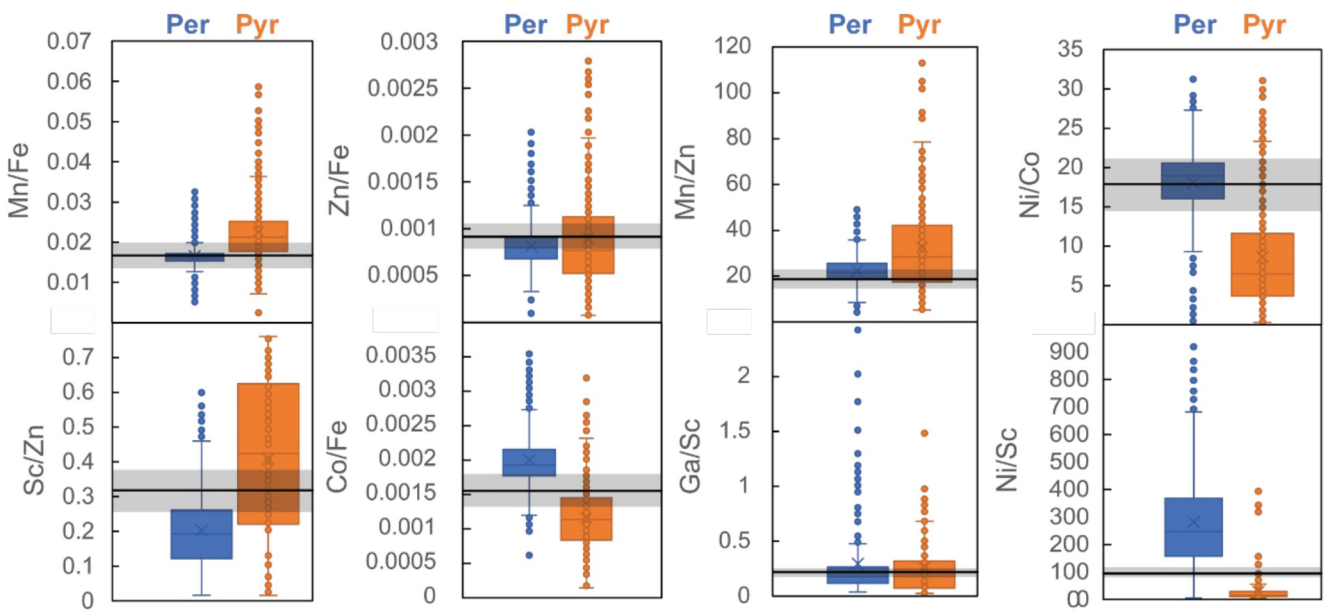

Figure C1. Box plots of elemental ratios for peridotite (blue) and pyroxenite (orange) data sets. Within each box, horizontal lines denote median values; boxes extend from the 25th to the 75th percentile of each group's distribution of values; vertical extending lines denote adjacent values (i.e., the most extreme values within 1.5 interquartile range of the 25th and 75th percentile of each group); dots denote observations outside the range of adjacent values. The solid black line and the associated gray box represent the R_0 value and its standard deviation (Table 1).

Conflict of Interest

The authors declare no conflicts of interest relevant to this study.

Data Availability Statement

Data and outputs of the models are shared in tables in the main text and as Tables S1–S8. Tables S1–S8 are available in Zenodo (Cunningham et al., 2026).

Acknowledgments
We would like to thank all crew, drilling team members, and lab technicians onboard the R/V JOIDES Resolution. This study benefited from discussions with Ananya Mallik, Lynne Elkins, Kevin Mendoza, and Stuart Kenderes. This work was supported by the U.S. Science Support Program, IODP, by the NSF Grants EAR-1946346 and EAR-2503705 to SL, and by the ACS Petroleum Research Fund Grant 61305-DNI8 to S.L. EHC also acknowledges support from the Schlanger Ocean Drilling Fellowship program and the University of Utah Graduate Research Fellowship program. SP and MTJ acknowledge the support of the Research Council of Norway through the PALMAR project no. 336293.

References

Asimow, P. D., & Ghiorso, M. S. (1998). Algorithmic modifications extending MELTS to calculate subsolidus phase relations. *American Mineralogist*, *83*(9–10), 1127–1132. https://doi.org/10.2138/am-1998-9-1022

Berndt, C., Planke, S., Alvestad, E., Tsikalas, F., & Rasmussen, T. (2001). Seismic volcanostratigraphy of the Norwegian Margin: Constraints on tectonomagmatic break-up processes. *Journal of the Geological Society*, *158*(3), 413–426. https://doi.org/10.1144/jgs.158.3.413

Bijwaard, H., & Spakman, W. (1999). Tomographic evidence for a narrow whole mantle plume below Iceland. *Earth and Planetary Science Letters*, *166*(3–4), 121–126. https://doi.org/10.1016/S0012-821X(99)00004-7

Borchardt, J. S., & Lee, C. T. (2022). Hot or fertile origin for continental break-up flood basalts: Insights from olivine systematics. *Lithosphere*, *2022*(1), 7161484. https://doi.org/10.2113/2022/7161484

Boutilier, R. R., & Keen, C. E. (1999). Small-scale convection and divergent plate boundaries. *Journal of Geophysical Research*, *104*(B4), 7389–7403. https://doi.org/10.1029/1998JB900076

Bowman, E. E., & Ducea, M. N. (2023). Pyroxenite melting at subduction zones. *Geology*, *51*(4), 383–386. https://doi.org/10.1130/G50929.1

Boyden, J. A., Müller, D. R., Gurnis, M., Torsvik, T. H., Clark, J. A., Turner, M., et al. (2011). Next-generation plate-tectonic reconstructions using GPlates. In G. R. Keller & C. Baru (Eds.), *Geoinformatics: Cyberinfrastructure for the Solid Earth Sciences* (pp. 95–114). Cambridge University Press. https://doi.org/10.1017/CBO9780511976308.008

Brandon, A. D., Graham, D. W., Waight, T., & Gautason, B. (2007). ^{186}Os and ^{187}Os enrichments and high- ^{3}He/^{4}He sources in the Earth's mantle: Evidence from Icelandic picrites. *Geochimica et Cosmochimica Acta*, *71*(18), 4570–4591. https://doi.org/10.1016/j.gca.2007.07.015

Breddam, K., Kurz, M. D., & Storey, M. (2000). Mapping out the conduit of the Iceland mantle plume with helium isotopes. *Earth and Planetary Science Letters*, *176*(1), 45–55. https://doi.org/10.1016/S0012-821X(99)00313-1

Brown, E. L., & Lesher, C. E. (2014). North Atlantic magmatism controlled by temperature, mantle composition and buoyancy. *Nature Geoscience*, *7*(11), 820–824. https://doi.org/10.1038/ngeo2264

Brueckner, H. K., & van Roermund, H. L. (2004). Dunk tectonics: A multiple subduction/eduction model for the evolution of the Scandinavian Caledonides. *Tectonics*, *23*(2). https://doi.org/10.1029/2003TC001502

Brune, S., Williams, S. E., Butterworth, N. P., & Müller, R. D. (2016). Abrupt plate accelerations shape rifted continental margins. *Nature*, *536*(7615), 201–204. https://doi.org/10.1038/nature18319

Cao, G., Tong, Y., Li, X., & Wang, L. (2022). Insights from olivine chemistry into crustal magmatic processes and the mantle source lithology of basalts from Hainan Island, China. *Lithos*, *430*, 106852. https://doi.org/10.1016/j.lithos.2022.106852

Celli, N. L., Lebedev, S., Schaeffer, A. J., & Gaina, C. (2021). The tilted Iceland Plume and its effect on the North Atlantic evolution and magmatism. *Earth and Planetary Science Letters*, *569*, 117048. https://doi.org/10.1016/j.epsl.2021.117048

Chauvel, C., & Hémond, C. (2000). Melting of a complete section of recycled oceanic crust: Trace element and Pb isotopic evidence from Iceland. *Geochemistry, Geophysics, Geosystems*, *1*(2), 1001. https://doi.org/10.1029/1999GC000002

Chen, C., Yao, Z. S., & Wang, C. Y. (2022). Partitioning behaviors of cobalt and manganese along diverse melting paths of peridotitic and MORB-like pyroxenitic mantle. *Journal of Petrology*, *63*(4), egac021. https://doi.org/10.1093/petrology/egac021

Chen, S., Wang, X. H., Niu, Y. L., Sun, P., Duan, M., Xiao, Y. Y., et al. (2017). Simple and cost-effective methods for precise analysis of trace element abundances in geological materials with ICP-MS. *Science Bulletin*, *62*(4), 277–289. https://doi.org/10.1016/j.scib.2017.01.004

Condamine, P., Couzinié, S., Fabbrizio, A., Devidal, J. L., & Médard, E. (2022). Trace element partitioning during incipient melting of phlogopite-peridotite in the spinel and garnet stability fields. *Geochimica et Cosmochimica Acta*, *327*, 53–78. https://doi.org/10.1016/j.gca.2022.04.011

Cunningham, E. H., Lambart, S., Guo, P., Chatterjee, S., Tegner, C., Hartley, A. H., et al. (2026). Evolution of the Source mineralogy and lithospheric controls on magmatism during the Northeast Atlantic continental breakup: Supplementary data tables. *Zenodo*. https://doi.org/10.5281/zenodo.15177255

Davis, F. A., Humayun, M., Hirschmann, M. M., & Cooper, R. S. (2013). Experimentally determined mineral/melt partitioning of first-row transition elements (FRTE) during partial melting of peridotite at 3GPa. *Geochimica et Cosmochimica Acta*, *104*, 232–260. https://doi.org/10.1016/j.gca.2012.11.009

Dekov, V. M., Rouxel, O., Asael, D., Hålenius, U., & Munnik, F. (2013). Native Cu from the oceanic crust: Isotopic insights into native metal origin. *Chemical Geology*, *359*, 136–149. https://doi.org/10.1016/j.chemgeo.2013.10.001

Duncan, R. A., Larsen, H. C., Allan, J. F., Aita, Y., Arndt, N. T., Bücker, C. J., et al. (1996). *Proceedings of the ODP, initial reports: Southeast Greenland margin, Ocean Drilling Program* (Vol. 163). https://doi.org/10.2973/odp.proc.ir.163.1996

Eason, D., & Sinton, J. (2006). Origin of high-Al N-MORB by fractional crystallization in the upper mantle beneath the Galapagos Spreading Center. *Earth and Planetary Science Letters*, *252*(3–4), 423–436. https://doi.org/10.1016/j.epsl.2006.09.048

Eldholm, O., Thiede, J., Taylor, E., Barton, C., Bjørklund, K., Bleil, U., et al. (1987). Summary and preliminary conclusions, ODP Leg 104. In O. Eldholm, J. Thiede, E. Taylor, C. Barton, K. Bjørklund, U. Bleil, et al. (Eds.), *Proceedings of the Ocean Drilling Program, Initial Reports* (Vol. 104, pp. 751–771). Ocean Drilling Program. https://doi.org/10.2973/odp.proc.ir.104.107.1987

Eldholm, O., Thiede, J., & Taylor, E. (1989). Evolution of the Vøring volcanic margin. In O. Eldholm, J. Thiede, E. Taylor, C. Barton, K. Bjørklund, U. Bleil, et al. (Eds.), *Proceedings of the Ocean Drilling Program, Scientific Results* (Vol. 104, pp. 1033–1065). Ocean Drilling Program. https://doi.org/10.2973/odp.proc.sr.104.191.1989

Ernst, R. E., Bond, D. P. G., Zhang, S., Buchan, K. L., Grasby, S. E., Youbi, N., et al. (2021). Large igneous province record through time and implications for secular environmental changes and geological time-scale boundaries. In R. E. Ernst, A. J. Dickson, & A. Bekker (Eds.), *Large Igneous Provinces: A Driver of Global Environmental and Biotic Changes* (pp. 1–26). https://doi.org/10.1002/9781119507444.ch1

Ezad, I. S., Shea, J. J., & Foley, S. F. (2025). Hydrous minerals are sinks for first row transition elements in the mantle: An experimental partitioning study. *Chemical Geology*, *690*, 122883. https://doi.org/10.1016/j.chemgeo.2025.122883

Fernández, M., Torne, M., Garcia-Castellanos, D., Vergés, J., Wheeler, W., & Karpuz, R. (2004). Deep structure of the Vøring Margin: The transition from a continental shield to a young oceanic lithosphere. *Earth and Planetary Science Letters*, *221*(1–4), 131–144. https://doi.org/10.1016/S0012-821X(04)00092-5

Fitton, J. G., Larsen, L. M., Saunders, A. D., Hardarson, B. S., & Kempton, P. D. (2000). Palaeogene continental to oceanic magmatism on the SE Greenland continental margin at 63°N: A review of the results of ocean drilling program legs 152 and 163. *Journal of Petrology*, *41*(7), 951–966. https://doi.org/10.1093/petrology/41.7.951

Fitton, J. G., Saunders, A. D., Norry, M. J., Hardarson, B. S., & Taylor, R. N. (1997). Thermal and chemical structure of the Iceland plume. *Earth and Planetary Science Letters*, *153*(3–4), 197–208. https://doi.org/10.1016/S0012-821X(97)00170-2

Foley, S. F., Ezad, I. S., Shu, C., & Förster, M. W. (2025). Melting of amphibole-apatite-rich metasomes in the continental mantle and comparison of melt compositions with natural igneous rocks. *Lithos*, *500–501*, 107976. https://doi.org/10.1016/j.lithos.2025.107976

Foulger, G. R., Natland, J. H., & Anderson, D. L. (2005). Genesis of the Iceland melt anomaly by plate tectonic processes. In G. R. Foulger, J. H. Natland, D. C. Presnall, & D. L. Anderson (Eds.), *Plates, Plumes and Paradigms* (Vol. 388, pp. 595–625). https://doi.org/10.1130/0-8137-2388-4.595

Fram, M. S., & Lesher, C. E. (1993). Geochemical constraints on mantle melting during creation of the North Atlantic basin. *Nature*, *363*(6431), 712–715. https://doi.org/10.1038/363712a0

Franke, D. (2013). Rifting, lithosphere breakup and volcanism: Comparison of magma-poor and volcanic rifted margins. *Marine and Petroleum Geology*, *43*, 63–87. https://doi.org/10.1016/j.marpetgeo.2012.11.003

French, S. W., & Romanowicz, B. (2015). Broad plumes rooted at the base of the Earth's mantle beneath major hotspots. *Nature*, *525*(7567), 95–99. https://doi.org/10.1038/nature14876

Gale, A., Dalton, C. A., Langmuir, C. H., Su, Y., & Schilling, J.-G. (2013). The mean composition of ocean ridge basalts. *Geochemistry, Geophysics, Geosystems*, *14*(3), 489–518. https://doi.org/10.1029/2012GC004334

Gernigon, L., Lucazeau, F., Brigaud, F., Ringenbach, J. C., Planke, S., & Le Gall, B. (2006). A moderate melting model for the Vøring margin (Norway) based on structural observations and a thermo-kinematical modelling: Implication for the meaning of the lower crustal bodies. *Tectonophysics*, *412*(3–4), 255–278. https://doi.org/10.1016/j.tecto.2005.10.038

Gernon, T. M., Barr, R., Fitton, J. G., Hincks, T. K., Keir, D., Longman, J., et al. (2022). Transient mobilization of subcrustal carbon coincident with Palaeocene–Eocene thermal maximum. *Nature Geoscience*, *15*(7), 573–579. https://doi.org/10.1038/s41561-022-00967-6

Ghiorso, M. S., & Sack, R. O. (1995). Chemical mass-transfer in magmatic processes IV. A revised and internally consistent thermodynamic model for the interpolation and extrapolation of liquid-solid equilibria in magmatic systems at elevated-temperatures and pressures. *Contributions to Mineralogy and Petrology*, *119*(2–3), 197–212. https://doi.org/10.1007/BF00307281

Gomes, A. S., & Vasconcelos, P. M. (2021). Geochronology of the Paraná-Etendeka large igneous province. *Earth-Science Reviews*, *220*, 103716. https://doi.org/10.1016/j.earscirev.2021.103716

Gómez-Ulla, A., Sigmarsson, O., & Gudfinnsson, G. H. (2017). Trace element systematics of olivine from historical eruptions of Lanzarote, Canary Islands: Constraints on mantle source and melting mode. *Chemical Geology*, *449*, 99–111. https://doi.org/10.1016/j.chemgeo.2016.11.021

Gorczyk, W., & Gonzalez, C. M. (2019). CO_2 degassing and melting of metasomatized mantle lithosphere during rifting–Numerical study. *Geoscience Frontiers*, *10*(4), 1409–1420. https://doi.org/10.1016/j.gsf.2018.11.003

Gurenko, A. A., Sobolev, A. V., Hoernle, K. A., Hauff, F., & Schmincke, H. U. (2009). Enriched, HIMU-type peridotite and depleted recycled pyroxenite in the Canary plume: A mixed-up mantle. *Earth and Planetary Science Letters*, *277*(3–4), 514–524. https://doi.org/10.1016/j.epsl.2008.11.013

Gurnis, M., Turner, M., Zahirovic, S., DiCaprio, L., Spasojevic, S., Müller, R., et al. (2012). Plate tectonic reconstructions with continuously closing plates. *Computers & Geosciences*, *38*(1), 35–42. https://doi.org/10.1016/j.cageo.2011.04.014

Hartley, R. A., Roberts, G. G., White, N., & Richardson, C. (2011). Transient convective uplift of an ancient buried landscape. *Nature Geoscience*, *4*(8), 562–565. https://doi.org/10.1038/ngeo1191

Harðardóttir, S., Matthews, S., Halldórsson, S. A., & Jackson, M. G. (2022). Spatial distribution and geochemical characterization of Icelandic mantle end-members: Implications for plume geometry and melting processes. *Chemical Geology*, *604*. https://doi.org/10.1016/j.chemgeo.2022.120930

Herzberg, C. (2011). Identification of source lithology in the Hawaiian and Canary Islands: Implications for origins. *Journal of Petrology*, *52*(1), 113–146. https://doi.org/10.1093/petrology/egq075

Herzberg, C., & Asimow, P. (2015). PRIMELT3 MEGA.XLSM software for primary magma calculation: Peridotite primary magma MgO contents from the liquidus to the solidus. *Geochemistry, Geophysics, Geosystems*, *16*(2), 563–578. https://doi.org/10.1002/2014GC005631

Herzberg, C., & Asimow, P. D. (2008). Petrology of some oceanic island basalts: PRIMELT2.XLS software for primary magma calculation. *Geochemistry, Geophysics, Geosystems*, *9*. https://doi.org/10.1029/2008GC002057

Hirschmann, M. M., & Stolper, E. M. (1996). A possible role for garnet pyroxenite in the origin of the "garnet signature" in MORB. *Contributions to Mineralogy and Petrology*, *124*(2), 185–208. https://doi.org/10.1007/s004100050184

Hofmann, A. W., Jochum, K. P., Seufert, M., & White, W. M. (1986). Nb and Pb in oceanic basalts: New constraints on mantle evolution. *Earth and Planetary Science Letters*, *79*(1–2), 33–45. https://doi.org/10.1016/0012-821X(86)90038-5

Holbrook, W. S., Larsen, H. C., Korenaga, J., Dahl-Jensen, T., Reid, I. D., Kelemen, P. B., et al. (2001). Mantle thermal structure and active upwelling during continental breakup in the North Atlantic. *Earth and Planetary Science Letters*, *190*(3–4), 251–266. https://doi.org/10.1016/S0012-821X(01)00392-2

Hole, M. J. (2018). Mineralogical and geochemical evidence for polybaric fractional crystallization of continental flood basalts and implications for identification of peridotite and pyroxenite source lithologies. *Earth-Science Reviews*, *176*, 51–67. https://doi.org/10.1016/j.earscirev.2017.09.014

Hole, M. J., & Millett, J. M. (2016). Controls of mantle potential temperature and lithospheric thickness on magmatism in the North Atlantic Igneous Province. *Journal of Petrology*, *57*(2), 417–436. https://doi.org/10.1093/petrology/egw014

Hole, M. J., & Natland, J. H. (2020). Magmatism in the North Atlantic Igneous Province; mantle temperatures, rifting and geodynamics. *Earth-Science Reviews*, *206*, 102794. https://doi.org/10.1016/j.earscirev.2019.02.011

Howarth, G. H., & Harris, C. (2017). Discriminating between pyroxenite and peridotite sources for continental flood basalts (CFB) in southern Africa using olivine chemistry. *Earth and Planetary Science Letters*, *475*, 143–151. https://doi.org/10.1016/j.epsl.2017.07.043

Huismans, R. S., & Beaumont, C. (2011). Depth-dependent extension, two-stage breakup and cratonic underplating at rifted margins. *Nature*, *473*(7345), 74–78. https://doi.org/10.1038/nature09988

Huismans, R. S., & Beaumont, C. (2014). Rifted continental margins: The case for depth-dependent extension. *Earth and Planetary Science Letters*, *407*, 148–162. https://doi.org/10.1016/j.epsl.2014.09.032

Humayun, M., Qin, L., & Norman, M. D. (2004). Geochemical evidence for excess iron in the mantle beneath Hawaii. *Science*, *306*(5693), 91–94. https://doi.org/10.1126/science.1101050

Hutton, J. (1788). *Theory of the Earth; or, an investigation of the laws observable in the composition, dissolution, and restoration of land upon the globe*. Transactions of the Royal Society of Edinburgh.

Jing, J. J., Su, B. X., Xiao, Y., Zhang, H. F., Uysal, İ., Chen, C., et al. (2019). Reactive origin of mantle harzburgite: Evidence from orthopyroxene-spinel association. *Lithos*, *342*, 175–186. https://doi.org/10.1016/j.lithos.2019.05.011

Jones, M. T., Jerram, D. A., Svensen, H. H., & Grove, C. (2016). The effects of large igneous provinces on the global carbon and sulphur cycles. *Palaeogeogaphy, Palaeoclimatology, Palaeoecology*, *441*, 4–21. https://doi.org/10.1016/j.palaeo.2015.06.042

Jones, M. T., Stokke, E. W., Rooney, A. D., Frieling, J., Pogge von Strandmann, P. A., Wilson, D. J., et al. (2023). Tracing North Atlantic volcanism and seaway connectivity across the Paleocene–Eocene thermal maximum (PETM). *Climate of the Past*, *19*(8), 1623–1652. https://doi.org/10.5194/cp-19-1623-2023

Keen, C. E., & Boutilier, R. R. (2000). Interaction of rifting and hot horizontal plume sheets at volcanic margins. *Journal of Geophysical Research*, *105*(B6), 13375–13387. https://doi.org/10.1029/2000JB900027

Kent, A. J. R., Stolper, E. M., Francis, D., Woodhead, J., Frei, R., & Eiler, J. (2004). Mantle heterogeneity during the formation of the North Atlantic igneous province: Constraints from trace element and Sr-Nd-Os-O isotope systematics of Baffin Island picrites. *Geochemistry, Geophysics, Geosystems*, *5*(11), Q11004. https://doi.org/10.1029/2004GC000743

King, S. D., & Anderson, D. L. (1995). An alternative mechanism of flood basalt formation. *Earth and Planetary Science Letters*, *136*(3–4), 269–279. https://doi.org/10.1016/0012-821X(95)00205-Q

King, S. D., & Anderson, D. L. (1998). Edge-driven convection. *Earth and Planetary Science Letters*, *160*(3–4), 289–296. https://doi.org/10.1016/S0012-821X(98)00089-2

Kiseeva, E. S., Fonseca, R. O. C., & Smythe, D. J. (2017). Chalcophile elements and sulfides in the upper mantle. *Elements*, *13*(2), 111–116. https://doi.org/10.2113/gselements.13.2.111

Kiseeva, E. S., & Wood, B. J. (2015). The effects of composition and temperature on chalcophile and lithophile element partitioning into magmatic sulphides. *Earth and Planetary Science Letters*, *424*, 280–294. https://doi.org/10.1016/j.epsl.2015.05.012

Klein, E. M., & Langmuir, C. H. (1987). Global correlations of ocean ridge basalt chemistry with axial depth and crustal thickness. *Journal of Geophysical Research*, *92*(B8), 8089–8115. https://doi.org/10.1029/JB092iB08p08089

Kogiso, T., Hirschmann, M. M., & Pertermann, M. (2004). High-pressure partial melting of mafic lithologies in the mantle. *Journal of Petrology*, *45*(12), 2407–2422. https://doi.org/10.1093/petrology/egh057

Koptev, A., & Cloetingh, S. (2024). Role of large igneous provinces in continental break-up varying from "shirker" to "producer". *Communications Earth & Environment*, *5*(1), 27. https://doi.org/10.1038/s43247-023-01191-9

Koptev, A., Cloetingh, S., & Ehlers, T. A. (2021). Longevity of small-scale ("baby") plumes and their role in lithospheric break-up. *Geophysical Journal International*, *227*(1), 439–471. https://doi.org/10.1093/gji/ggab223

Korenaga, J. (2004). Mantle mixing and continental breakup magmatism. *Earth and Planetary Science Letters*, *218*(3–4), 463–473. https://doi.org/10.1016/S0012-821X(03)00674-5

Korenaga, J., Holbrook, W. S., Kent, G. M., Kelemen, P. B., Detrick, R. S., Larsen, H. C., & Dahl Jensen, T. (2000). Crustal structure of the southeast Greenland margin from joint refraction and reflection seismic tomography. *Journal of Geophysical Research*, *105*, 21591–21614. https://doi.org/10.1016/S0012-821X(00)00308-3

Korenaga, J., & Kelemen, P. B. (2000). Major element heterogeneity in the mantle source of the North Atlantic igneous province. *Earth and Planetary Science Letters*, *184*(1), 251–268. https://doi.org/10.1016/S0012-821X(00)00308-3

Korenaga, J., Kelemen, P. B., & Holbrook, W. S. (2002). Methods for resolving the origin of large igneous provinces from crustal seismology. *Journal of Geophysical Research*, *107*(B9), 2178. https://doi.org/10.1029/2001JB001030

Kurz, M. D., Meyer, P. S., & Sigurdsson, H. (1985). Helium isotopic systematics within the neovolcanic zones of Iceland. *Earth and Planetary Science Letters*, *74*(4), 291–305. https://doi.org/10.1016/S0012-821X(85)80001-7

Lambart, S., Baker, M. B., & Stolper, E. M. (2016). The role of pyroxenite in basalt genesis: Melt-PX, a melting parameterization for mantle pyroxenites between 0.9 and 5 GPa. *Journal of Geophysical Research: Solid Earth*, *121*(8), 5708–5735. https://doi.org/10.1002/2015JB012762

Lambart, S., Laporte, D., & Schiano, P. (2013). Markers of the pyroxenite contribution in the major-element compositions of oceanic basalts: Review of the experimental constraints. *Lithos*, *160–161*, 14–36. https://doi.org/10.1016/j.lithos.2012.11.018

Lang, O. I., & Lambart, S. (2022). First-row transition elements in pyroxenites and peridotites: A promising tool for constraining mantle source mineralogy. *Chemical Geology*, *612*, 121137. https://doi.org/10.1016/j.chemgeo.2022.121137

Larsen, H. C., Duncan, R. A., Allan, J. F., & Brooks, K. (1999). *Proceedings of the ocean drilling program, scientific results* (Vol. 163). Ocean Drilling Program. https://doi.org/10.2973/odp.proc.sr.163.1999

Larsen, H. C., & Saunders, A. D. (1998). Tectonism and volcanism at the southeast Greenland rifted margin: A record of plume impact and later continental rupture. In A. D. Saunders, H. C. Larsen, & S. W. Wise (Eds.), *Proceedings of the Ocean Drilling Program, Scientific Results* (Vol. 152, pp. 503–533). Ocean Drilling Program. https://doi.org/10.2973/odp.proc.sr.152.240.1998

Larsen, H. C., Saunders, A. D., Clift, P. D., Ali, J. R., Begét, J., Cambray, H., et al. (1994). *Proc. ODP, Init. Repts* (Vol. 152). Ocean Drilling Program. https://doi.org/10.2973/odp.proc.ir.152.1994

Larsen, L. M., & Pedersen, A. K. (2000). Processes in high-Mg, high-T magmas: Evidence from olivine, chromite and glass in Palaeogene picrites from West Greenland. *Journal of Petrology*, *41*(7), 1071–1098. https://doi.org/10.1093/petrology/41.7.1071

Larsen, L. M., & Pedersen, A. K. (2009). Petrology of the Paleocene picrites and flood basalts on Disko and Nuussuaq, West Greenland. *Journal of Petrology*, *50*(9), 1667–1711. https://doi.org/10.1093/petrology/egp048

Lawver, L. A., & Müller, R. D. (1994). Iceland hotspot track. *Geology*, *22*(4), 311–314. https://doi.org/10.1130/0091-7613(1994)022<0311:iht>2.3.co;2

Lee, C. T. A., Leeman, W. P., Canil, D., & Li, Z. X. A. (2005). Similar V/Sc systematics in MORB and arc basalts: Implications for the oxygen fugacities of their mantle source regions. *Journal of Petrology*, *46*(11), 2313–2336. https://doi.org/10.1093/petrology/egi056

Lee, C. T. A., Luffi, P., Plank, T., Dalton, H., & Leeman, W. (2009). Constraints on the depths and temperatures of basaltic magma generation on Earth and other terrestrial planets using new thermobarometers for mafic magmas. *Earth and Planetary Science Letters*, *279*(1–2), 20–33. https://doi.org/10.1016/j.epsl.2008.12.020

LeHuray, A. P. (1989). Native copper in ODP Site 642 tholeiites. In *Proceedings of the Ocean Drilling Program, Scientific Results, College Station* (Vol. 104, pp. 411–417). Ocean Drilling Program.

Le Roux, V., Dasgupta, R., & Lee, C. T. A. (2011). Mineralogical heterogeneities in the Earth's mantle: Constraints from Mn, Co, Ni and Zn partitioning during partial melting. *Earth and Planetary Science Letters*, *307*(3–4), 395–408. https://doi.org/10.1016/j.epsl.2011.05.014

Le Roux, V., Dasgupta, R., & Lee, C. T. A. (2015). Recommended mineral-melt partition coefficients for FRTEs (Cu), Ga, and Ge during mantle melting. *American Mineralogist*, *100*(11–12), 2533–2544. https://doi.org/10.2138/am-2015-5215

Le Roux, V., Lee, C. T. A., & Turner, S. J. (2010). Zn/Fe systematics in mafic and ultramafic systems: Implications for detecting major element heterogeneities in the Earth's mantle. *Geochimica et Cosmochimica Acta*, *74*(9), 2779–2796. https://doi.org/10.1016/j.gca.2010.02.004

Li, Z. X., & Lee, C. T. (2004). The constancy of upper mantle fO2 through time inferred from V/Sc ratios in basalts. *Earth and Planetary Science Letters*, *228*, 483–493. https://doi.org/10.1016/j.epsl.2004.10.00

Lu, G., & Huismans, R. S. (2021). Melt volume at Atlantic volcanic rifted margins controlled by depth-dependent extension and mantle temperature. *Nature Communications*, *12*(1), 3894. https://doi.org/10.1038/s41467-021-23981-5

Mallik, A., Lambart, S., & Chin, E. J. (2021). Tracking the evolution of magmas from heterogeneous mantle sources to eruption. In J. Konter, M. Ballmer, S. Cottaar, & H. Marquardt (Eds.), *Mantle Convection and Surface Expressions* (pp. 151–177). AGU Books. https://doi.org/10.1002/9781119528609.ch6

Marty, B., Upton, B. G. J., & Ellam, R. M. (1998). Helium isotopes in early Tertiary basalts, northeast Greenland: Evidence for 58 Ma plume activity in the North Atlantic—Iceland volcanic province. *Geology*, *26*(5), 407–410. https://doi.org/10.1130/0091-7613(1998)026<0407:hiietb>2.3.co;2

Marzoli, A., Callegaro, S., Corso, J. D., Davies, J. H. F. L., Chiaradia, M., Youbi, N., et al. (2018). The Central Atlantic Magmatic Province (CAMP): A review. In L. H. Tanner (Ed.), *The Late Triassic World*, *Topics in Geobiology* (Vol. 46, pp. 91–125). https://doi.org/10.1007/978-3-319-68009-5_4

McKenzie, D., & Bickle, M. J. (1988). The volume and composition of melt generated by extension of the lithosphere. *Journal of Petrology*, *29*(3), 625–697. https://doi.org/10.1093/petrology/29.3.625

Médard, E., Schmidt, M. W., Schiano, P., & Ottolini, L. (2006). Melting of amphibole-bearing wehrlites: An experimental study on the origin of ultra-calcic nepheline-normative melts. *Journal of Petrology*, *47*(3), 481–504. https://doi.org/10.1093/petrology/egi083

Meyer, R., Hertogen, J., Pedersen, R. B., Viereck-Götte, L., & Abratis, M. (2009). Interaction of mantle derived melts with crust during the emplacement of the Vøring Plateau, NE Atlantic. *Marine Geology*, *261*(1–4), 3–16. https://doi.org/10.1016/j.margeo.2009.02.007

Millett, J. M., Hole, M. J., Jolley, D. W., Passey, S. R., & Rossetti, L. (2020). Transient mantle cooling linked to regional volcanic shut-down and early rifting in the North Atlantic Igneous Province. *Bulletin of Volcanology*, *82*(8), 61. https://doi.org/10.1007/s00445-020-01401-8

Mjelde, R., & Faleide, J. I. (2009). Variation of Icelandic and Hawaiian magmatism: Evidence for co-pulsation of mantle plumes? *Marine Geophysical Researches*, *30*(1), 61–72. https://doi.org/10.1007/S11001-009-9066-0

Mjelde, R., Raum, T., Breivik, A., Shimamura, H., Murai, Y., Takanami, T., & Faleide, J. I. (2005). Crustal structure of the Vøring Margin, NE Atlantic: A review of geological implications based on recent OBS data. *Geological Society of London, Petroleum Geology Conference Series*, *6*(1), 803–813. https://doi.org/10.1144/0060803

Montelli, R., Nolet, G., Dahlen, F. A., Masters, G., Engdahl, E. R., & Hung, S. H. (2004). Finite-frequency tomography reveals a variety of plumes in the mantle. *Science*, *303*(5656), 338–343. https://doi.org/10.1126/science.1092485

Morgan, W. J. (1971). Convection plumes in the lower mantle. *Nature*, *230*(5288), 42–43. https://doi.org/10.1038/230042a0

Morris, A. M., Lambart, S., Stearns, M. A., Bowman, J. R., Jones, M. T., Mohn, G., et al. (2024). Evidence for low-pressure crustal anatexis during the Northeast Atlantic break-up. *Geochemistry, Geophysics, Geosystems*, *25*(7), e2023GC011413. https://doi.org/10.1029/2023GC011413

Mourey, A. J., Shea, T., Lynn, K. J., Lerner, A. H., Lambart, S., Costa, F., et al. (2022). Trace elements in olivine fingerprint the source of 2018 magmas and shed light on explosive-effusive eruption cycles at Kīlauea Volcano. *Earth and Planetary Science Letters*, *595*, 117769. https://doi.org/10.1016/j.epsl.2022.117769

Murton, B. J., Taylor, R. N., & Thirlwall, M. F. (2002). Plume–ridge interaction: A geochemical perspective from the Reykjanes Ridge. *Journal of Petrology*, *43*(11), 1987–2012. https://doi.org/10.1093/petrology/43.11.1987

Mutter, J. C., Buck, W. R., & Zehnder, C. M. (1988). Convective partial melting: 1. A model for the formation of thick basaltic sequences during the initiation of spreading. *Journal of Geophysical Research*, *93*(B2), 1031–1048. https://doi.org/10.1029/JB093iB02p01031

Nielsen, T. K., & Hopper, J. R. (2004). From rift to drift: Mantle melting during continental breakup. *Geochemistry, Geophysics, Geosystems*, *5*(7), Q07003. https://doi.org/10.1029/2003GC000662

Nirrengarten, M., Gernigon, L., & Manatschal, G. (2014). Lower crustal bodies in the Møre volcanic rifted margin: Geophysical determination and geological implications. *Tectonophysics*, *636*, 143–157. https://doi.org/10.1016/j.tecto.2014.08.004

Niu, Y. (2025). Shallow origin of continental mantle materials beneath slow-spreading ocean ridges. *Science Bulletin*, *70*(10), 1533–1537. https://doi.org/10.1016/j.scib.2025.01.028

Oliveira, A. L., Hollanda, M. H. B., Schmitz, M. D., Macêdo Filho, A. A., Erba, E., & Crowley, J. L. (2025). High-precision geochronology of the Equatorial Atlantic Magmatic Province (EQUAMP): Temporal correlations with the Paraná-Etendeka Magmatic Province and the Weissert Event. *Earth and Planetary Science Letters*, *658*, 119330. https://doi.org/10.1016/j.epsl.2025.119330

Parnell-Turner, R., White, N., Henstock, T., Murton, B., Maclennan, J., & Jones, S. M. (2014). A continuous 55-million-year record of transient mantle plume activity beneath Iceland. *Nature Geoscience*, *7*(12), 914–919. https://doi.org/10.1038/ngeo2281

Péron-Pinvidic, G., Manatschal, G., & IMAGinING RIFTING" Workshop Participants. (2019). Rifted margins: State of the art and future challenges. *Frontiers in Earth Science*, *7*, 218. https://doi.org/10.3389/feart.2019.00218

Pertermann, M., & Hirschmann, M. M. (2003). Partial melting experiments on a MORB-like pyroxenite between 2 and 3 GPa: Constraints on the presence of pyroxenite in basalt source regions from solidus location and melting rate. *Journal of Geophysical Research*, *108*(B2), 2125. https://doi.org/10.1029/2000JB000118

Petersen, K. D., Schiffer, C., & Nagel, T. (2018). LIP formation and protracted lower mantle upwelling induced by rifting and delamination. *Scientific Reports*, *8*(1), 1–11. https://doi.org/10.1038/s41598-018-34194-0

Pilet, S. (2015). Generation of low-silica alkaline lavas: Petrological constraints, models, and thermal implications. In G. R. Foulger, M. Lustrino, & S. D. King (Eds.), *The Interdisciplinary Earth: A Volume in Honor of Don L. Anderson*, *Geological Society of America Special Paper 514 and America Geophysical Union Special Publication* (Vol. 71, pp. 281–304). https://doi.org/10.1130/2015.2514

Pilet, S., Baker, M. B., & Stolper, E. M. (2008). Metasomatized lithosphere and the origin of alkaline lavas. *Science*, *320*(5878), 916–919. https://doi.org/10.1126/science.1156563

Pin, J., France, L., Lambart, S., & Reisberg, L. (2022). Thermodynamic modeling of melt addition to peridotite: Implications for the refertilization of the non-cratonic continental mantle lithosphere. *Chemical Geology*, *609*, 121050. https://doi.org/10.1016/j.chemgeo.2022.121050

Plank, T., & Langmuir, C. H. (1998). The chemical composition of subducting sediment and its consequences for the crust and mantle. *Chemical Geology*, *362*(6422), 739–743. https://doi.org/10.1016/S0009-2541(97)00150-2

Planke, S., Berndt, C., Alvarez Zarikian, C. A., Agarwal, A., Andrews, G. D. M., Betlem, P., et al. (2023a). Expedition 396 summary. In S. Planke, C. Berndt, C. A. Alvarez Zarikian, & the Expedition 396 Scientists (Eds.), *Mid-Norwegian Margin Magmatism and Paleoclimate Implications*, *Proceedings of the International Ocean Discovery Program* (Vol. 396). International Ocean Discovery Program. https://doi.org/10.14379/iodp.proc.396.101.2023

Planke, S., Berndt, C., Alvarez Zarikian, C. A., Agarwal, A., Andrews, G. D. M., Betlem, P., et al. (2023b). Site U1566. In S. Planke, C. Berndt, C. A. Alvarez Zarikian, & the Expedition 396 Scientists (Eds.), *Mid-Norwegian Margin Magmatism and Paleoclimate Implications*, *Proceedings of the International Ocean Discovery Program* (Vol. 396). International Ocean Discovery Program. https://doi.org/10.14379/iodp.proc.396.104.2023

Planke, S., Berndt, C., Alvarez Zarikian, C. A., Agarwal, A., Andrews, G. D. M., Betlem, P., et al. (2023c). Sites U1571 and U1572. In S. Planke, C. Berndt, C. A. Alvarez Zarikian, & the Expedition 396 Scientists (Eds.), *Mid-Norwegian Margin Magmatism and Paleoclimate Implications*, *Proceedings of the International Ocean Discovery Program* (Vol. 396). International Ocean Discovery Program. https://doi.org/10.14379/iodp.proc.396.107.2023

Planke, S., Berndt, C., Alvarez Zarikian, C. A., Agarwal, A., Andrews, G. D. M., Betlem, P., et al. (2023d). Site U1574. In S. Planke, C. Berndt, C. A. Alvarez Zarikian, & the Expedition 396 Scientists (Eds.), *Mid-Norwegian Margin Magmatism and Paleoclimate Implications*, *Proceedings of the International Ocean Discovery Program* (Vol. 396). International Ocean Discovery Program. https://doi.org/10.14379/iodp.proc.396.109.2023

Planke, S., Berndt, C., Alvarez Zarikian, C. A., Agarwal, A., Andrews, G. D. M., Betlem, P., et al. (2023e). Site U1573. In S. Planke, C. Berndt, C. A. Alvarez Zarikian, & the Expedition 396 Scientists (Eds.), *Mid-Norwegian Margin Magmatism and Paleoclimate Implications*, *Proceedings of the International Ocean Discovery Program* (Vol. 396). International Ocean Discovery Program. https://doi.org/10.14379/iodp.proc.396.108.2023

Planke, S., Berndt, C., Alvarez Zarikian, C. A., Agarwal, A., Andrews, G. D. M., Betlem, P., et al. (2023f). Expedition 396 methods. In S. Planke, C. Berndt, C. A. Alvarez Zarikian, & the Expedition 396 Scientists (Eds.), *Mid-Norwegian Margin Magmatism and Paleoclimate Implications*, *Proceedings of the International Ocean Discovery Program* (Vol. 396). International Ocean Discovery Program. https://doi.org/10.14379/iodp.proc.396.102.2023

Planke, S., Berndt, C., Alvarez Zarikian, C. A., Bünz, S., Zastrozhnov, D., Lebedeva-Ivanova, N. N., et al. (2023). The Nature of Outer Highs on Volcanic Rifted Margins: Results from High-Resolution Seismic Data and IODP Drilling on the Vøring Margin, Norwegian Sea. In *AGU Fall Meeting Abstracts* (Vol. 1297, pp. OS11C–1297).

Planke, S., Rasmussen, T., Rey, S., & Myklebust, R. (2005). Seismic characteristics and distribution of volcanic intrusions and hydrothermal vent complexes in the Vøring and Møre basins. In A. G. Doré & B. A. Vining (Eds.), *Petroleum Geology: North-West Europe and Global Perspectives—Proceedings of the 6th Petroleum Geology Conference* (pp. 833–844). Geological Society. https://doi.org/10.1144/0060833

Planke, S., Symonds, P. A., Alvestad, E., & Skogseid, J. (2000). Seismic volcanostratigraphy of large-volume basaltic extrusive complexes on rifted margins. *Journal of Geophysical Research*, *105*, B8. https://doi.org/10.1029/1999JB900005

Prytulak, J., & Elliott, T. (2007). TiO2 enrichment in ocean island basalts. *Earth and Planetary Science Letters*, *263*(3–4), 388–403. https://doi.org/10.1016/j.epsl.2007.09.015

Qin, L., & Humayun, M. (2008). The Fe/Mn ratio in MORB and OIB determined by ICP-MS. *Geochimica et Cosmochimica Acta*, *72*(6), 1660–1677. https://doi.org/10.1016/j.gca.2008.01.012

Rateau, R., Schofield, N., & Smith, M. (2013). The potential role of igneous intrusions on hydrocarbon migration, West of Shetland. *Petroleum Geoscience*, *19*(3), 259–272. https://doi.org/10.1144/petgeo2012-035

Reynolds, P., Planke, S., Millett, J. M., Jerram, D. A., Trulsvik, M., Schofield, N., & Myklebust, R. (2017). Hydrothermal vent complexes offshore Northeast Greenland: A potential role in driving the PETM. *Earth and Planetary Science Letters*, *467*, 72–78. https://doi.org/10.1016/j.epsl.2017.03.031

Ribe, N. M., Christensen, U. R., & Theiging, J. (1995). The dynamics of plume-ridge interaction, 1: Ridge-centered plumes. *Earth and Planetary Science Letters*, *134*(1–2), 155–168. https://doi.org/10.1016/0012-821X(95)00116-T

Ritsema, J., Heijst, H. J. V., & Woodhouse, J. H. (1999). Complex shear wave velocity structure imaged beneath Africa and Iceland. *Science*, *286*(5446), 1925–1928. https://doi.org/10.1126/science.286.5446.1925

Rooney, T. O., Brown, E. L., Bastow, I. D., Arrowsmith, J. R., & Campisano, C. J. (2023). Magmatism during the continent–ocean transition. *Earth and Planetary Science Letters*, *614*, 118189. https://doi.org/10.1016/j.epsl.2023.118189

Rosenthal, A., Foley, S. F., Pearson, D. G., Nowell, G. M., & Tappe, S. (2009). Petrogenesis of strongly alkaline primitive volcanic rocks at the propagating tip of the western branch of the East African Rift. *Earth and Planetary Science Letters*, *284*(1–2), 236–248. https://doi.org/10.1016/j.epsl.2009.04.036

Salters, V. J. M., & Stracke, A. (2004). Composition of the depleted mantle. *Geochemistry, Geophysics, Geosystems*, *5*(5), Q05B07. https://doi.org/10.1029/2003GC000597

Saunders, A. D., Fitton, J. G., Kerr, A. C., Norry, M. J., & Kent, R. W. (1997). The North Atlantic igneous province. In J. J. Mahoney & M. F. Coffin (Eds.), *Large Igneous Provinces: Continental, Oceanic, and Planetary Flood Volcanism* (Vol. 100, pp. 45–93). American Geophysical Union Geophysical Monograph. https://doi.org/10.1029/GM100p0045

Saunders, A. D., Larsen, H. C., & Wise, S. W. Jr. (Eds.) (1998)., *Proceedings of the Ocean Drilling Program, Scientific Results* (Vol. 152). Ocean Drilling Program. https://doi.org/10.2973/odp.proc.sr.152.1998

Schilling, J. G. (1973). Iceland mantle plume: Geochemical study of Reykjanes Ridge. *Nature*, *242*(5400), 565–571. https://doi.org/10.1038/242565a0

Schilling, J. G. (1991). Fluxes and excess temperatures of mantle plumes inferred from their interaction with migrating mid-ocean ridges. *Nature*, *352*(6334), 397–403. https://doi.org/10.1038/352397a0

Senda, R., Kimura, J. I., & Chang, Q. (2014). Evaluation of a rapid, effective sample digestion method for trace element analysis of granitoid samples containing acid-resistant minerals: Alkali fusion after acid digestion. *Geochemical Journal*, *48*(1), 99–103. https://doi.org/10.2343/geochemj.2.0280

Shellnutt, J. G., & Pham, T. T. (2018). Mantle potential temperature estimates and primary melt compositions of the low-Ti Emeishan flood basalt. *Frontiers in Earth Science*, *6*, 67. https://doi.org/10.3389/feart.2018.00067

Shorttle, O., Maclennan, J., & Lambart, S. (2014). Quantifying lithological variability in the mantle. *Earth and Planetary Science Letters*, *395*, 24–40. https://doi.org/10.1016/j.epsl.2014.03.040

Simon, K., Huismans, R. S., & Beaumont, C. (2009). Dynamical modeling of lithospheric extension and small-scale convection: Implications for magmatism during the formation of volcanic rifted margins. *Geophysical Journal International*, *176*(1), 327–350. https://doi.org/10.1111/j.1365-246X.2008.03891.x

Skogseid, J., Planke, S., Faleide, J. I., Pedersen, T., Eldholm, O., & Neverdal, F. (2000). NE Atlantic continental rifting and volcanic margin formation. *Geological Society - Special Publications*, *167*(1), 295–326. https://doi.org/10.1144/GSL.SP.2000.167.01.12

Smith, P. M., & Asimow, P. D. (2005). Adiabat_1ph: A new public front-end to the MELTS, pMELTS, and pHMELTS models. *Geochemistry, Geophysics, Geosystems*, *6*(2), Q02004. https://doi.org/10.1029/2004GC000816

Sobolev, A. V., Hofmann, A. W., Kuzmin, D. V., Yaxley, G. M., Arndt, N. T., Chung, S. L., et al. (2007). The amount of recycled crust in sources of mantle-derived melts. *Science*, *316*(5823), 412–418. https://doi.org/10.1126/science.1138113

Sobolev, A. V., Hofmann, A. W., Sobolev, S. V., & Nikogosian, I. K. (2005). An olivine-free mantle source of Hawaiian shield basalts. *Nature*, *434*(7033), 590–597. https://doi.org/10.1038/nature03411

Spice, H. E., Fitton, J. G., & Kirstein, L. A. (2016). Temperature fluctuation of the Iceland mantle plume through time. *Geochemistry, Geophysics, Geosystems*, *17*(2), 243–254. https://doi.org/10.1002/2015GC006059

Starkey, N. A., Stuart, F. M., Ellam, R. M., Fitton, J. G., Basu, S., & Larsen, L. M. (2009). Helium isotopes in early Iceland plume picrites: Constraints on the composition of high $^{3}He/^{4}He$ mantle. *Earth and Planetary Science Letters*, *277*(1–2), 91–100. https://doi.org/10.1016/j.epsl.2008.10.007

Steinberger, B., Bredow, E., Lebedev, S., Schaeffer, A., & Torsvik, T. H. (2019). Widespread volcanism in the Greenland–North Atlantic region explained by the Iceland plume. *Nature Geoscience*, *12*(1), 61–68. https://doi.org/10.1038/s41561-018-0251-0

Storey, M., Duncan, R. A., & Swisher, C. C., III. (2007). Paleocene-Eocene thermal maximum and the opening of the northeast Atlantic. *Science*, *316*(5824), 587–589. https://doi.org/10.1126/science.1135274

Storey, M., Duncan, R. A., & Tegner, C. (2007). Timing and duration of volcanism in the North Atlantic Igneous Province: Implications for geodynamics and links to the Iceland hotspot. *Chemical Geology*, *241*(3–4), 264–281. https://doi.org/10.1016/j.chemgeo.2007.01.016

Stracke, A., & Béguelin, P. (2024). Basalts record a limited extent of mantle depletion: Cause and chemical geodynamic implications. *Geochemical Perspectives Letters*, *32*, 21–26. https://doi.org/10.7185/geochemlet.2437

Straub, S. M., LaGatta, A. B., Martin-Del Pozzo, A. L., & Langmuir, C. H. (2008). Evidence from high-Ni olivines for a hybridized peridotite/pyroxenite source for orogenic andesites from the central Mexican Volcanic Belt. *Geochemistry, Geophysics, Geosystems*, *9*(3), Q03007. https://doi.org/10.1029/2007GC001583

Stuart, F., Lass-Evans, S., Godfrey Fitton, J., & Ellam, R. M. (2003). High $^{3}He/^{4}He$ ratios in picritic basalts from Baffin Island and the role of a mixed reservoir in mantle plumes. *Nature*, *424*(6944), 57–59. https://doi.org/10.1038/nature01711

Talwani, M., & Eldholm, O. (1977). Evolution of the Norwegian-Greenland Sea. *Geological Society of America Bulletin*, *88*(7), 969–999. https://doi.org/10.1130/0016-7606(1977)88<969:eotns>2.0.co;2

Talwani, M., Udintsev, G. B., & White, S. M. (1976). Introduction and Explanatory Notes, Leg 38, Deep Sea Drilling Project. In *Deep Sea Drilling Project* (Vol. 38, pp. 3–19). https://doi.org/10.2973/dsdp.proc.38.1976

Tegner, C., Guo, P., Chatterjee, S., Lambart, S., Jones, M. T., Planke, S., et al. (2025). New geochemical analyses on samples drilled on the mid-Norwegian margin during IODP Expedition 396, ODP Leg 104 and DSDP Leg 38. *GFZ Data Services*. https://doi.org/10.5880/digis.2025.011

Tegner, C., Lesher, C. E., Larsen, L. M., & Watt, W. S. (1998). Evidence from the rare-earth-element record of mantle melting for cooling of the tertiary Iceland plume. *Nature*, *395*(6702), 591–594. https://doi.org/10.1038/26956

Thirwall, M. F., Gee, M. A. M., Taylor, R. N., & Murton, B. J. (2004). Mantle compositions in Iceland and adjacent ridges investigated using double-spike Pb isotope ratios. *Geochimica et Cosmochimica Acta*, *68*(2), 361–386. https://doi.org/10.1016/S0016-7037(03)00424-1

Torsvik, T. H., Amundsen, H. E., Trønnes, R. G., Doubrovine, P. V., Gaina, C., Kusznir, N. J., et al. (2015). Continental crust beneath southeast Iceland. *Proceedings of the National Academy of Sciences of the United States of America*, *112*(15), E1818–E1827. https://doi.org/10.1073/pnas.1423099112

Usui, T., Righter, K., Shearer, C. K., & Jones, J. H. (2022). Effect of sulfur on siderophile element partitioning between olivine and a primary melt from the Martian mantle. *American Mineralogist*, *107*(3), 357–368. https://doi.org/10.2138/am-2021-7743

van den Bleeken, G., Müntener, O., & Ulmer, P. (2011). Melt variability in percolated peridotite: An experimental study applied to reactive migration of tholeiitic basalt in the upper mantle. *Contributions to Mineralogy and Petrology*, *161*(6), 921–945. https://doi.org/10.1007/s00410-010-0572-5

Veter, M., Foley, S. F., Mertz-Kraus, R., & Groschopf, N. (2017). Trace elemens in olivine of ultramafic lamprophyres controlled by phlogopite-rich mineral assemblages in the mantle source. *Lithos*, *292–294*, 81–95. https://doi.org/10.1016/j.lithos.2017.08.020

Viereck, L. G., Hertogen, J., Parson, L. M., Morton, A. C., Love, D., & Gibson, I. L. (1989). Chemical stratigraphy and petrology of the Vøring Plateau: Theoleiitic lavas and interlayered volcaniclastic sediments at ODP Hole 642E. In O. Eldholm, J. Thiede, & E. Taylor (Eds.), *Proceedings of the Ocean Drilling Program, Scientific Results* (pp. 367–396). Ocean Drilling Program.

Viereck, L. G., Taylor, P. N., Parson, L. M., Morton, A. C., Hertogen, J., Gibson, I. L., & the ODP Leg 104 Scientific Party. (1988). Origin of the Palaeogene Vøring Plateau volcanic sequence. *Geological Society, London, Special Publications*, *39*(1), 69–83. https://doi.org/10.1144/gsl.sp.1988.039.01.08

Vogt, P. R. (1983). The Iceland mantle plume: Status of the hypothesis after a decade of New Work. In M. H. P. Bott, S. Saxov, M. Talwani, & J. Thiede (Eds.), *Structure and Development of the Greenland-Scotland Ridge. Nato Conference Series* (Vol. 8, pp. 191–213). Springer. https://doi.org/10.1007/978-1-4613-3485-9_11

Walter, M. J. (1998). Melting of garnet peridotite and the origin of komatiite and depleted lithosphere. *Journal of Petrology*, *39*(1), 29–60. https://doi.org/10.1093/petroj/39.1.29

Wangen, M., Fjeldskaar, W., Faleide, J. I., Wilson, J., Zweigel, J., & Austegard, A. (2008). Forward modeling of stretching episodes and paleo heat flow of the Vøring margin, NE Atlantic. *Journal of Geodynamics*, *45*(2–3), 83–98. https://doi.org/10.1016/j.jog.2007.07.002

White, R., & McKenzie, D. (1989). Magmatism at rift zones: The generation of volcanic continental margins and flood basalts. *Journal of Geophysical Research*, *94*(B6), 7685–7729. https://doi.org/10.1029/JB094iB06p07685

White, R. S. (1988). A hot-spot model for early Tertiary volcanism in the N Atlantic. *Geological Society - Special Publications*, *39*(1), 3–13. https://doi.org/10.1144/GSL.SP.1988.039.01.02

Wilkinson, C., Ganerød, M., Hendriks, B., & Eide, E. (2017). Compilation and appraisal of geochronological data from the North Atlantic Igneous Province (NAIP). In G. Péron-Pinvidic, J. R. Hopper, M. S. Stoker, C. Gaina, J. C. Doornenbal, T. Funck, et al. (Eds.), *The NE Atlantic Region: A Reappraisal of Crustal Structure, Tectonostratigraphy and Magmatic Evolution*. Geological Society, London, Special Publications.

Willhite, L. N., Jackson, M. G., Blichert-Toft, J., Bindeman, I., Kurz, M. D., Halldórsson, S. A., et al. (2019). Hot and Heterogenous High - $^{3}He/^{4}He$ Component: New constraints from proto-Iceland plume lavas from Baffin Island. *Geochemistry, Geophysics, Geosystems*, *20*, 5939–5967. https://doi.org/10.1029/2019GC008654

Wolfe, C. J., Bjarnason, I. T., VanDecar, J. C., & Solomon, S. C. (1997). Seismic structure of the Iceland mantle plume. *Nature*, *385*(6613), 245–247. https://doi.org/10.1038/385245a0

Xu, R., Liu, Y., & Lambart, S. (2020). Melting of a hydrous peridotite mantle source under the Emeishan large igneous province. *Earth-Science Reviews*, *207*, 103253. https://doi.org/10.1016/j.earscirev.2020.103253

Yang, Z. F., Li, J., Jiang, Q. B., Xu, F., Guo, S. Y., Li, Y., & Zhang, J. (2019). Using Major element log ratios to recognize compositional patterns of basalt: Implications for source lithological and compositional heterogeneities. *Journal of Geophysical Research: Solid Earth*, *124*(4), 3458–3490. https://doi.org/10.1029/2018JB016145

Yang, Z. F., & Zhou, J. H. (2013). Can we identify source lithology of basalt? *Scientific Reports*, *3*(1), 1856. https://doi.org/10.1038/srep01856

Zahirovic, S., Eleish, A., Doss, S., Pall, J., Cannon, J., Pistone, M., et al. (2022). Subduction and carbonate platform interactions. *Geoscience Data Journal*, *9*(2), 371–383. https://doi.org/10.1002/gdj3.146

Zhang, G. L., Zong, C. L., Yin, X. B., & Li, H. (2012). Geochemical constraints on a mixed pyroxenite–peridotite source for East Pacific Rise basalts. *Chemical Geology*, *330*, 176–187. https://doi.org/10.1016/j.chemgeo.2012.08.033

References From the Supporting Information

Abdelmalak, M. M., Meyer, R., Planke, S., Faleide, J. I., Gernigon, L., Frieling, J., et al. (2016). Pre-breakup magmatism on the Vøring Margin: Insight from new sub-basalt imaging and results from Ocean Drilling Program Hole 642E. *Tectonophysics*, *675*, 258–274. https://doi.org/10.1016/j.tecto.2016.02.037

Allen, R. M., Nolet, G., Morgan, W. J., Vogfjörd, K., Bergsson, B. H., Erlendsson, P., et al. (1999). The thin hot plume beneath Iceland. *Geophysical Journal International*, *137*(1), 51–63. https://doi.org/10.1046/j.1365-246x.1999.00753.x

Asimow, P. D., & Langmuir, A. C. (2003). The importance of water to oceanic mantle melting regimes. *Nature*, *421*(6925), 815–820. https://doi.org/10.1038/nature01429

Berman, R. G., & Koziol, A. M. (1991). Ternary excess properties of grossular-pyrope-almandine garnet and their influence in geothermobarometry. *American Mineralogist*, *76*(7–8), 1223–1231.

Boulter, M. C., & Manum, S. B. (1989). The Brito-Arctic igneous province flora around the Paleocene/Eocene boundary. In O. Eldholm, J. Thiede, E. Taylor, C. Barton, K. Bjørklund, U. Bleil, et al. (Eds.), *Proceedings of the Ocean Drilling Program, Scientific Results* (Vol. 104, pp. 663–680).

Dasgupta, R., & Hirschmann, M. M. (2006). Melting in the Earth's deep upper mantle caused by carbon dioxide. *Nature*, *440*(7084), 659–662. https://doi.org/10.1038/nature04612

Fram, M. S., & Lesher, C. E. (1997). Generation and polybaric differentiation of East Greenland Early Tertiary flood basalts. *Journal of Petrology*, *38*(2), 231–275. https://doi.org/10.1093/petroj/38.2.231

Gernigon, L., Knies, J., Schönenberger, J., Piraquive, A., van Der Lelij, R., Huyskens, M. H., et al. (2024). Understanding volcanic margin evolution through the lens of Norway's youngest granite. *Terra Nova*, *36*(4), 250–257. https://doi.org/10.1111/ter.12705

Ghiorso, M. S., & Sack, R. O. (1991). Fe-Ti oxide geothermometry: Thermodynamic formulation and the estimation of intensive variables in silicic magmas. *Contributions to Mineralogy and Petrology*, *108*(4), 485–510. https://doi.org/10.1007/BF00303452

Gradstein, F. M., Ogg, J. G., & Hilgen, F. J. (2012). On the geologic time scale. *Newsletters on Stratigraphy*, *45*(2), 171–188. https://doi.org/10.1127/0078-0421/2012/0020

Hou, Y. S., Li, H. Y., Wang, Y., Zhang, Y. F., Li, Y., & Xu, Y. G. (2024). Experimental insights into the petrogenesis of plume-related magmas: Tholeiite-harzburgite interaction at 2–3 GPa and 1,400–1,500 C. *Journal of Geophysical Research: Solid Earth*, *129*(7), e2023JB028467. https://doi.org/10.1029/2023JB028467

Katz, R. F., Spiegelman, M., & Langmuir, C. H. (2003). A new parameterization of hydrous mantle melting. *Geochemistry, Geophysics, Geosystems*, *4*(9), 1073. https://doi.org/10.1029/2002GC000433

Niu, Y., Regelous, M., Wendt, I. J., Batiza, R., & O'Hara, M. J. (2002). Geochemistry of near-EPR seamounts: Importance of source vs. process and the origin of enriched mantle component. *Earth and Planetary Science Letters*, *199*(3), 327–345. https://doi.org/10.1016/S0012-821X(02)00591-5

Niu, Y., & O'Hara, M. J. (2003). Origin of ocean island basalts: A new perspective from petrology, geochemistry, and mineral physics considerations. *Journal of Geophysical Research*, *108*, 2209. https://doi.org/10.1029/2002JB002048

Phipps Morgan, J. (2001). Thermodynamics of pressure release melting of a veined plum pudding mantle. *Geochemistry, Geophysics, Geosystems*, *2*(4), 1001. https://doi.org/10.1029/2000GC000049

Planke, S., Millett, J. M., Maharjan, D., Jerram, D. A., Mansour Abdelmalak, M., Groth, A., et al. (2017). Igneous seismic geomorphology of buries lava fields and coastal escarpments on the Vøring volcanic rifted margin. *Interpretation*, *5*(3), SK161–SK177. https://doi.org/10.1190/INT-2016-0164.1

Presnall, D. C., & Gudfinnsson, G. H. (2011). Oceanic volcanism from the low-velocity zone–without mantle plumes. *Journal of Petrology*, *52*(7–8), 1533–1546. https://doi.org/10.1093/petrology/egq093

Quanshi, Y., & Xuefa, S. (2014). Petrologic perspectives on tectonic evolution of a nascent basin (Okinawa Trough) behind Ryukyu Arc: A review. *Acta Oceanologica Sinica*, *33*(4), 1–12. https://doi.org/10.1007/s13131-014-0400-2

Ribe, N. M., Tackley, P. J., & Sanan, P. (2020). The strength of the Iceland plume: A geodynamical scaling approach. *Earth and Planetary Science Letters*, *551*, 116570. https://doi.org/10.1016/j.epsl.2020.116570

Richards, M. A., Duncan, R. A., & Courtillot, V. E. (1989). Flood basalts and hot-spot tracks: Plume heads and tails. *Science*, *246*(4926), 103–107. https://doi.org/10.1126/science.246.4926.103

Rudnick, R. L., & Gao, S. (2003). Composition of the continental crust. In H. D. Holland & K. K. Turekian (Eds.), *Treatise on Geochemistry* (Vol. 3, pp. 1–64). 08-043751-6/03016-4. https://doi.org/10.1016/b0

Steinberger, B., & Antretter, M. (2006). Conduit diameter and buoyant rising speed of mantle plumes: Implications for the motion of hot spots and shape of plume conduits. *Geochemistry, Geophysics, Geosystems*, *7*(11), Q11018. https://doi.org/10.1029/2006GC001409

Sun, S. S., & McDonough, W. F. (1989). Chemical and isotopic systematics of oceanic basalts: Implications for mantle composition and processes. *Geological Society - Special Publications*, *42*(1), 313–345. https://doi.org/10.1144/GSL.SP.1989.042.01.19

Walker, G. P. L. (1987). Pipe vesicles in Hawaiian basaltic lavas: Their origin and potential as paleoslope indicators. *Geology*, *15*(1), 84–87. https://doi.org/10.1130/0091-7613(1987)15<84:PVIHBL>2.0.CO;2